Sinkhole formation GIS-based mapping and geo-statistical prediction analysis in Chania area, Crete

by

Sofia Peleli

CHANIA JUNE 2019

Master's Thesis

Remote Sensing

Geoinformatics

Sinkhole formation GIS-based mapping and geostatistical prediction analysis in Chania area, Crete

by

Peleli Sofia

2018 - 2019

Supervisor:

Kouli Maria

to obtain the degree of Master of Science in Applied Earth Sciences (Geoenvironmental Resources & Risks) at the Hellenic Mediterranean University

UNESCO Chair
SOLID EARTH PHYSICS and GEOHAZARDS RISK REDUCTION
Technological Educational Institute of Crete, Greece
Head of the Chair, Dr. Filippos Vallianatos
Professor of Geophysics & Seismology
3 Romanou Str., Chania, GR 73100, Crete, Greece. email : fvallian@chania.teicrete.gr

ABSTRACT

The last years many researches have been done to evaluate sinkhole formation and to produce sinkhole susceptibility maps using the probability method of frequency ratio for prediction analysis. By determining the vulnerable areas it is possible to decrease the probability of damage caused by sinkholes in urban and agricultural areas. The purpose of this study is at first to create an accurate sinkhole inventory map in the study area and secondly to make a prediction analysis by producing a sinkhole susceptibility index based on the frequency ratio method within a geographic information system environment. For sinkhole formation inventory map, two TanDEM-X DEMs with a spatial resolution of 11.1m and 30m respectively were adapted. Six filters (area, depth, eccentricity, circularity index, proximity to streams & proximity to roads) were applied on initial sinkholes identification of each DEM to exclude falsely-identified depressions. Finally two sinkhole inventory maps were produced with 1038 sinkholes for the 11-meter TanDEM-X and 428 for the 30-meter TanDEM-X, showing that the 11-meter DEM is able to identify more sinkholes due to its better spatial resolution. The inventory map of the 11-meter TanDEM-X DEM was chosen for the prediction analysis. Sinkholes were separated in the training sinkhole dataset (70%) and the test sinkhole dataset (30%) and twelve sinkhole formation controlling factors; geology (lithology), hydrogeology, soils depth, slope, elevation, groundwater exploitation, distance & density to faults, distance &density to deep wells, drainage density and land use were chosen and analyzed for the sinkhole susceptibility index, which was classified in four classes; low, moderate, high & very high susceptibility. The sinkhole susceptibility map shows that 83.3% of the test sinkhole dataset fall within the “high” and “very high” susceptibility zones.

ACKNOWLEDGEMENTS

I would first like to thank my supervisor dr. Maria Kouli for all the help and the knowledge that she has provided me for more than 5 years. I am totally grateful for all the support that she has provided me with especially in some very tough moments and for the trust that she has showed to me. Without her guidance this Thesis may have never been completed.

I would also like to thank the professors who were involved in the validation survey for this research project and who are the second readers of this thesis: prof. Fillipos Valianatos and prof. Vasilis Saltas. Their advices and comments were useful for this study.

Special thanks to the bachelor students Rania Stivaktaki and Odysseas Aplathas for the support and help that gave me when I needed during the writing of this Thesis.

Last but not least, I must express my very profound gratitude and love to my parents, to my friends and to my partner, for providing me with unfailing support and continuous encouragement throughout my years of study and through the process of researching and writing this thesis. This accomplishment would not have been possible without them.

Peleli Sofia

Table of Contents

No table of figures entries found.

Fig.17: *Susceptibility maps of factors; distance to deep wells (top) and distance to faults (bottom)*

Fig.18: *Susceptibility maps of factors; deep wells' density (top) and elevation (bottom)*

Fig.19: *Susceptibility maps of factors; faults' density (top) and groundwater exploitation (bottom)*

Fig.20: *Susceptibility maps of factors; hydrogeology (top) and land use (bottom)*

Fig.21: *Susceptibility maps of factors; soil depth (top) and slope gradient (bottom)*

Fig.22: *Map of Sinkhole Susceptibility Index*

Fig.23: *Pictures that show the spatial distribution of sinkholes' test dataset with the sinkhole susceptibility map. Dark blue color refers to "very high" class.*

LIST OF TABLES

INTRODUCTION

Sinkhole formation is one of the most damaging hazards in karst terrains. In such karst environments, geomorphology and hydrology, both at the surface and in the subsurface, are governed by dissolution of carbonate rocks resulting to enclosed depressions (dolines or sinkholes and poljes), swallow holes and large springs. Karst setting can be bare, covered or mantled and interstratal, depending on whether the soluble rocks are exposed at the surface, covered by unconsolidated deposits or overlain by non-karst rocks, respectively.

Mapping of the karst features is essential for multiple health and safety reasons since many properties (structures, fields, parks etc.) are damaged or are completely destroyed every year in all over the world especially by cover-collapse sinkholes. In some cases whole towns have been called to be abandoned by the authorities. Furthermore more there are large impacts on the local economy by the damages of these events.

Since the field surveys, especially in large scales, are very expensive and in some cases it is very difficult to approach the studying area due to the land's geomorphology, the need of alternative ways of studying the soil erosion is in high demand. Remote sensing techniques and GIS mapping offer multiple products and tools for this aim along with new methods.

The aim of this study is first to identify the already existed sinkholes in the karstic area of Chania, Crete, by using two Digital Elevation Model datasets (the two TAN-DEM-X). In a next step, the sinkhole susceptibility analysis is implemented using the method of frequency ratio. The 70% of the sinkholes included in the inventory map is used to evaluate the importance of several sinkhole-controlling factors. Frequency ratio method is based on the observed associations between distribution of sinkholes and each controlling factor display the correlation between sinkhole locations and the parameters controlling sinkhole occurrence in the area.

Finally, a sinkhole susceptibility map is generated in order to reveal areas prone to sinkhole formation and its performance is tested using the rest 30% of the sinkholes inventory map.

CHAPTER 1 SINKHOLES, NATURE & CHARACTERISTICS

1.1 Theoretical Background

A sinkhole is a depression on the surface of the ground due to the dissolution or sudden collapse of surface sediments into bedrock cavities[1]. Sinkholes form in different shapes (shallow bowls, saucers or have vertical walls) and may reach hundreds of meters in diameter and depth. Usually their formation id happening very slowly, during the pass of many years, but in some cases this creation happens fast due to sudden collapse of the surface (fig.1). When it rains, the water stays inside the sinkhole and usually drains into the subsurface, but if the soil contains a large amount of clay, natural ponds might be formed since the water is not able to pass into the ground. Sinkholes are met mostly in karstic terrains or in probably underground karstic terrains.

Karstic terrain consists mostly by limestone, carbonates, gypsum or dolomites and refers to the region where the bedrock may be dissolved by slightly acidic groundwater [1]. A main characteristic of the karstic terrains is the presence features such as springs, caves, dry streams and sinkholes (fig.1). Approximately the 13% of the world's land surface is characterized by karst. [2]

Slightly acidic water is created by the absorption of carbon dioxide from air and soils. The features are a result of the acidic water that dissolves the bedrock and forms conduits in the rock, which carry water from the surface to springs located in valleys (fig.2). Eventually, these conduits become exposed by erosion and if they are enough big, a cave formation is being observed. Conduits are also called underground rivers because they have an area where the water collects and supplies the flow, like basins in surface rivers and might vary from a few hundred square meters to hundreds of square kilometers, to springs where it rises to the surface to join the more typical stream and river system. Sinkholes form into recharge area, in which the surface water is flowing into the subsurface and entering a conduit.

$CaCO3 + H2O + CO2$ (dissolved) $Ca+2 + 2HCO3-$

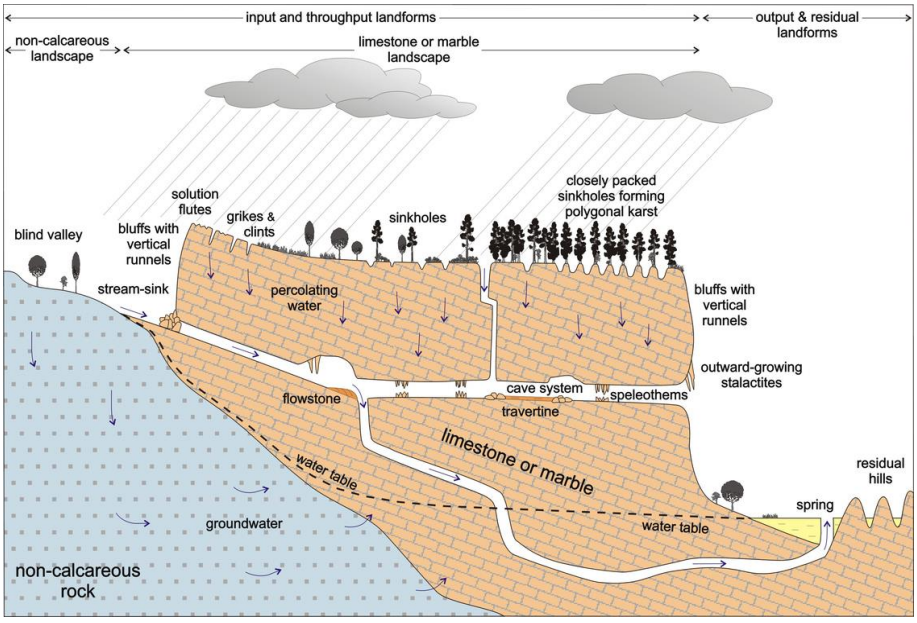

Fig.1: *Features and relationships associated with karst landscapes [3]*

1.2. Sinkhole formation system

One of the most common causes of sinkhole formation is the collapse of voids which naturally takes place in carbonate rocks [4]. Slightly acidic water is being created by the reaction of the carbon dioxide that exists in the atmosphere with rain water, which encounters with the rain in the soluble bedrock and is gradually dissolved along horizontal and vertical cracks and voids mainly along joints. More acidic water then starts encountering in the soluble bedrock and so the joints and cracks enlarge overtime with small soil particles are carried off. Soil sinks gradually, forming small depressions above the conduit and subsequently, the overburden subsides or collapses into the cavities forming depressions (sinkholes or dolines) at the surface [1]. The formation is a process that might be happening (enlarging) for many decades, or that might occur in just a moment from a sudden collapse.

Types of sinkholes;

Several genetic classifications of sinkholes have been proposed [5] [6] [7] [8];

Solution sinkholes; Formed by the differential corrosional lowering of the ground-surface where karst rocks are exposed at the surface or at bare karst formations [4]. These sinkholes are prone to be formed when the focused centripetal flow is governed toward higher permeability zones in the epikarst [9].

Subsidence sinkholes are consisting of a wide spectrum of dolines that are created by the dissolution of the subsurface, by the deformation and/or by the internal erosion of the undermined overlying material. The covering sediments are permeable and contain sand. These type of sinkholes can be described by two descriptors;(i) Cover, bed-rock or caprock which describe the material that is affected by erosion in the in the interior ground and/or by the deformation processes (fig.2), (ii)Collapse, suffosion, or sagging that describe the main type of retreat process (fig.2) [4].

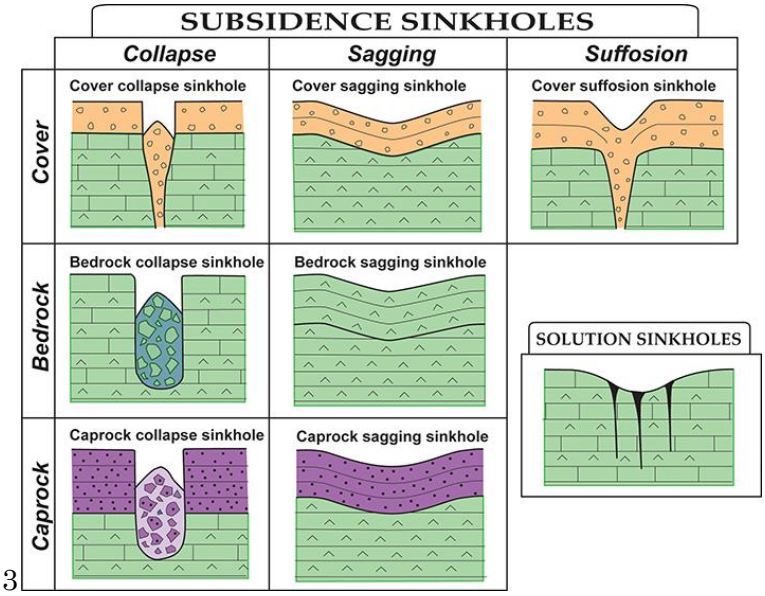

3

Figure 2: *Genetic classification of sinkholes showing each descriptor*

Sagging sinkholes Mantled karst refers to regions where the dissolvable bedrock is covered by unconsolidated cover deposits. It appears in the boundaries of the depositson the surface as an irregular rockhead covered by a folded cover with basin structures [10].

Cover-collapse sinkholes refer to the result of complex processes that occur through a succession of steps in karst terrains that are covered with a thick and loose sedimentary cover. Usually these sedimentary cover ranges in thickness between a few meters and approximately 30m [11]. They form mainly in recharge regions of covered karst terrains, or in regions of groundwater recharge.

Human-collapse sinkholes refer to sinkholes that are formed due to anthropogenic activity in the area. Deep wells, mines, induced seismicity are some of the causes of the human-collapse sinkholes. Other causes that refer to the change of the amount of

water that flows into the subsurface are the water pumping from deep wells, altered drainage from construction, and urban constructions such as streets and parking lots.

1.2.1. Sinkhole formation factors

The processes involved in the formation of sinkholes may be activated or accelerated by natural and anthropogenic changes in the karst environment [10]. The main factors that control sinkhole formation are:

- Composition of the karst rocks (lithology, mineralogy) and that of the adjacent lithologies. Karstification is often particularly intense when it is in contact non-karst rocks or above them [10].
- The structure (discontinuity planes, dip, folding, faults) and texture (grain size, porosity) of the karst rock leads to dissolution of the ground [10].Displacements along faults may guide to a high fracture density around and between faults increasing the soil's permeability, and so will increase the entrance and the flow of the water in the bedrock [12]. Because of this sinkholes and dolines might be created along the fault planes or in a close distance by the fault lineaments [12] [15] [16] [17] [18], and also these depressions are getting larger and migrated upward with the pass of the time when they exist at fault intersections.
- The amount of water and its physicochemical properties (saturation index, pH, temperature, alkalinity) that flows in the soluble rock affect the solubility of carbonate, which is mainly controlled by the dissolved CO derived from the atmosphere and the soil. Another fact is that groundwater may experience renewed aggressiveness due to mixing and temperature changes [10].
- Hydro-geological and hydrodynamic conditions, like gradient, hydraulic conductivity, phreatic or vadose, laminar or turbulent, strongly influence the dissolution kinetics, especially in high-solubility rocks. Static water in contact with salts rapidly becomes saturated with the consequent cessation of the transport-controlled dissolution process. The transition from laminar to turbulent flow involves a significant increase in the dissolution rate due to thinning of the diffusion boundary layer [10]. It is also noticed that sinkholes are denser in areas that large groundwater fluctuations exist. Mines, deep

wells and urban constructions also change these hydrodynamic conditions by groundwater pumping or because the water can enter to the subsurface through them.

- Ground characteristics, such as slope and elevation. There is an apparent topographic correlation, with sinkholes usually formed in elevated and flat (<5 degrees slope) areas [17].A difference in sinkhole frequency was clearly evident, with flat slopes containing more sinkholes than steep slopes. This finding was expected. Farrant and Cooper [22] suggested that dissolution pipes and irregular rockhead form on flat slopes, ideal for karst formation, whereas steep slopes promote erosion. This finding is additionally supported in the context of landslides in Glade [23] and Cooper [24], where steep slopes induce ground instability and consequential rockfall, thus also causing erosion indirectly. About elevation, [25] does note that exposed limestone initiates rapid recharge for sinkholes, so perhaps it is this indirect correlation that can cause a certain type of sinkhole; namely solution sinkholes (UWSP, n.d.)

- The soil in a sinkhole might be similar to the sand in the upper chamber of an hour-glass, ready to slip down through the constriction into the space below if disturbed [36]. Vegetation is often a main factor of soil's stability for two reasons. Because the roots of the trees help the soil to be more stable and because transpiration by the vegetation reduces the amount of water that would otherwise be able to flush soil grains down into the karst [26]. If vegetation is absent, more water gets underground, increasing the potential to collapse of the soil plug in the top of the cavity. Holes left after removing rotten tree roots or burnt trees might increase the entrances of water in the karst.

1.2.2. Why is important to monitor sinkholes

Sinkhole activity is not only a problematic natural process, but also a human-induced hazard [10]. The most dangerous sinkholes are the subsidence sinkholes due to their development that involves the deformation of the ground [10]. When sinkholes are created near infrastructure may cause major damage to roads, structural foundations, fields and utilities. In May 2012, a heavy rainfall event triggered 41 sinkholes at Maohe village, China, damaging 143 houses (69 collapsed), leading 1,830 citizens to relocate from the village [27]. In August 2012 a 450-meter sinkhole developed in the

swampy marshland near the rural community of Bayou Corne in Assumption Parish (i.e., county), Louisiana forced the citizens to abandoned the area. Some residents have still not been able to return while the sinkhole keeps growing and thus it is being monitored by multiple systems, including four rapid-response GPS continuously operating reference stations (CORS) called CORS911 [28].

The climatic change affects the sinkhole occurrence due to the rising of the temperatures, which will change natural hydrological processes [29], enhance dissolution of limestone [30] and promote soil failure [31]. In Chania Prefecture the two-month period of January-February of year 2019 was characterized by unprecedented phenomena of runoff, changing the natural hydrological processes of the area along with the presence of many landslides and sinkholes formation.

Fig.3a: *Photographs showing the sinkhole in Schmalkalden that opened up on 1 November 2010. It is 26 to 30 m in diameter and 12 to 17 m in depth [32] (b) Sinkhole in Trikala, Greece [33]*

Fig.*3b*: *Picture of Vothonas sinkhole field with water, Chania, Greece (picture taken by Thomas Panagiotou)*

In Chania there is a famous large sinkhole that is called Vothonas (fig.3b). The "area" of Vothonas is considered as one of the most fertile grounds in the region, due to the existence of huge amounts' of groundwater. The year 2019, because of the high precipitation, the sinkhole was filled with water, having as a result the local news to refer to it in the articles as "Lake Vothonas". The area keeps sinking and enlarging overtime and thus no houses built there, only fields. The sinkhole was successfully identified in this study case and it can be seen at figure 21 (left image)

1.3. Sinkhole Susceptibility, Hazard, and Risk Assessment and Prediction Analysis

"The past and present is the key to the future"

Uniformitarianism

The uniformitarian principle indicates that the behavior of nature is regular and indicative of an objective causal structure in which operative causes of the present may be shown into the past in order to explain the physical world in terms of historical development and projected into the future for prediction and control. The general assumption is that the fundamental causal regularities of the physical world have not changed over time and this can be proved by processing and inferring the past causes from presently observable effects [34]. Sinkhole inventories, along with the data of controlling factors of sinkhole development can be used as the basis to predict the spatial and temporal distribution of future sinkholes and their characteristics. Prediction is based on past events, where the underlying working hypothesis is that future sinkholes will have similar distribution patterns to the past ones. Ideally, each sinkhole type should be analyzed separately, due to their uniqueness, being possibly affected by different factors and have different distribution patterns and scaling relationships [10].

Depending on the information available, two types of models exist that are able to predict the occurrence of future sinkholes: (i) susceptibility models and (ii) hazard

models. Susceptibility models represent the probability of a sinkhole to occur in any specific place in terms of relative probability (high, medium, low) [10].

CHAPTER 2STUDY AREA & DATA

2.1. Study Area

The area that was selected for this study is the central and north part of Chania Prefecture. It belongs to Crete Island in Greece. It is located between 23.4° and 23.2° west-east longitudes and 35.4° and 35.5° north-south latitudes with a total area of 1336km^2 and it consists of four municipalities (Apokoronas, Chania, Platanias and Kissamos) (fig.4). According to the last census at 2011 [35], population of Chania Prefecture is 156,585 in total and of those 149,113 people live in the municipalities that were mentioned before. The two main activities of the area are agriculture and tourism. Until about 20 years ago apart from the main town of Chania the rest of the region were used mostly for agricultural and farming activities. Since over4.000.000 tourists visit the island every summer the last 2 years, these last two decades quite a lot of these land fields have turned into accommodations and other tourist facilities. The area is hilly with a lot of elevation changes in very small distances and it involves a part of one of the most unique karst basins worldwide, the Lefka Ori (White Mountains) that reach up to 2,453m altitude and cover an area of 800m^2. The mountain forms several large plateaus, located at heights of 500–1,100m (e.g. Omalos plateau, 1,080m) [37] and many gorges. In Chania region exist approximately 1500 caves and more than 60 gorges, out of the almost 400 that exist in all Crete island. North of Lefka Ori to the coastline of the island is a wide in which several rivers pass that springing from the fountains of the Lefka Ori Mountains. The intricate terrain of the north coast is characterized by four large mountainous peninsulas and among them sizeable gulfs [37]. The main land covers are agriculture, residential, semi-natural habitats and barren areas (fig.5 (bottom))

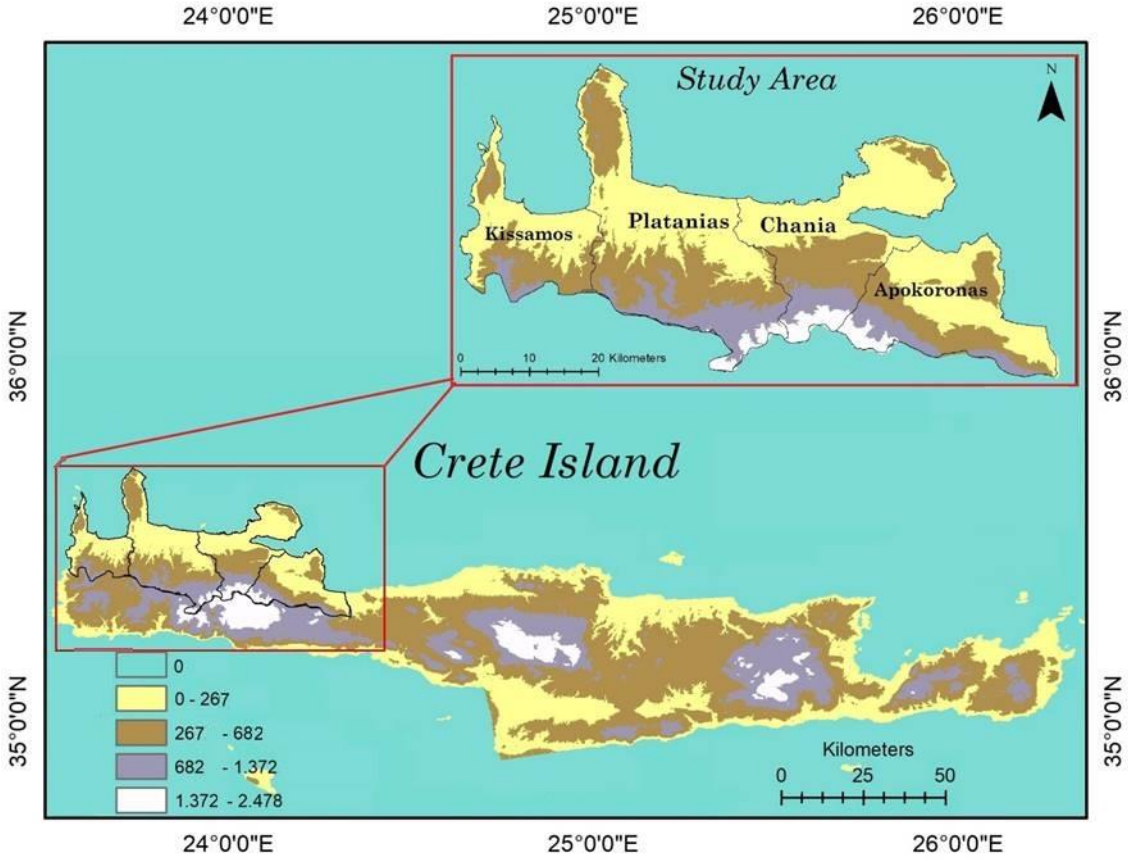

Figure 4: *Crete Island and the study area from TanDEM-X DEM of 11.1m spatial resolution.*

2.1.1. Climate and Meteorological characteristics

The climate is sub-humid Mediterranean with humid and relatively cold winters and dry and warm summers [38]. The area is considered as a semi-arid region with average annual precipitationof665 mm, of which 65% it is estimated to be lost in evapotranspiration, 21% as runoff to sea and only 14% recharges the groundwater [5]. The precipitation is not uniformly distributed throughout the year, since from May to October it is considered as a drought period. Thus precipitation is mainly concentrated from November to April. Some years extreme weather phenomena occur at the area. According to HNMS report for the year 2019 the monthly rainfall was 497mm was 72% of the average annual rainfall (approximately 310mm) for both June and February. The weather station in the area of Kastelli recorded 269mm of rain, which is 270% of the average February monthly rainfall. At this year the very intense

precipitation caused destructive flash floods in river basins, many landslides on slopes and disastrous damages at roads, fields and monuments.

2.1.2. Geological and hydro-geological characteristics of the study area

Crete Island is characterized by an extremely complicated geological structure with an intensive tectonic fragmentation [39]. The island constitutes of repeated tectonic covers consisting of variant geotectonic zones, which are a result of geological series [39].The faults in the study area have NW–SE and E–W directions [37].

More specifically, the study area is characterized by the following seven geological formations (fig.5 (top));

- **loose Quaternary deposits** Consist of alluvial deposits, terra rossa, clays and weathered materials from the erosion of calcitic rocks [7]. Quaternary deposits forming depositional plains are met mostly at the northern part of the study area, as well as along the coast line [39].

- **Neogene deposits;** mainly consists of marly limestones, marls, sandstones and clays [40]. Miocene to Pliocene sediments are found in the central and the northwestern part of the study area [37].

- **Tripolis and Trypalion carbonates;** Carbonates of the Trypalion nappe, which are exposed in the central-eastern part of the study area, extending from the north to the south, with a NE–SW direction [39].

- **Phylites – Quartzites;** Excavated hills of phyllites and quartzites, a late Carboniferous to late Triassic package of sedimentary rocks consisted mainly of quartz-rich silica clastic sediments, with small limestone, gypsum, and volcanic rocks, covering the central part of the study area [39].

- **Plattenkalk limestones;** Limestones of the Plattenkalk zone are mainly exposed to the most southeastern part of the study area [39].

- **Flysch;** Layers of sedimentary rocks that are characterized by the progress from deep-water and turbidity flow deposits to shallow-water shales and sandstones. They are found in a small area at the west Chania Prefecture.

The clouds that are approaching the island from the west side cannot easily pass the high Lefka Ori and thus many rainfalls occur in the region gathering great amounts of underground water and having streams connected to the drainage basin with their orientation being from west to east. From a hydro-lithological point of view, this is also a reason why the geological formations are classified into eight hydro-lithological units [9]: (fig.13 (top))

- Medium to low permeability rocks, which consists of karstic limestones and dolomites
- High to medium permeability rocks, which comprise the karstic limestones of Tripolis and Trypalion nappes and dolomites. Water movement is accomplished through the fracture zones and the chaotic karstic system. A high groundwater potential is expected and usually discharged by means of karstic springs [9];
- Low to very low permeability formations consist of Pliocene and Miocene marls and other impermeable Neogene formations [9];
- Fluctuant permeability formations consist mainly of recent to present alluvial deposits, eluvial mantle materials, fluvial deposits, talus cones, dunes and conglomerates in places. A shallow and low-potential aquifer is expected due to its interaction with surface water flows [9];
- Medium to high permeability formations, which consist mainly of Miocene and Pliocene deposits (Neogene marly limestones and conglomerates)
- medium to low permeability formations, which consist mainly of Miocene and Pliocene deposits (Neogene marly limestones and conglomerates) [9];
- Low to very low permeability formations, which are mainly composed of metamorphic rocks (phyllites, etc.), rocks of all the geological units and nappes (including the Ionion nappe). In some cases aquifers of high potential can be found [9], depending on the fracturing or the composition
- Low to very low permeability formations, which are mainly composed of metamorphic (phyllites, etc.) and rocks of all the geological units and nappes (including the Ionion nappe).

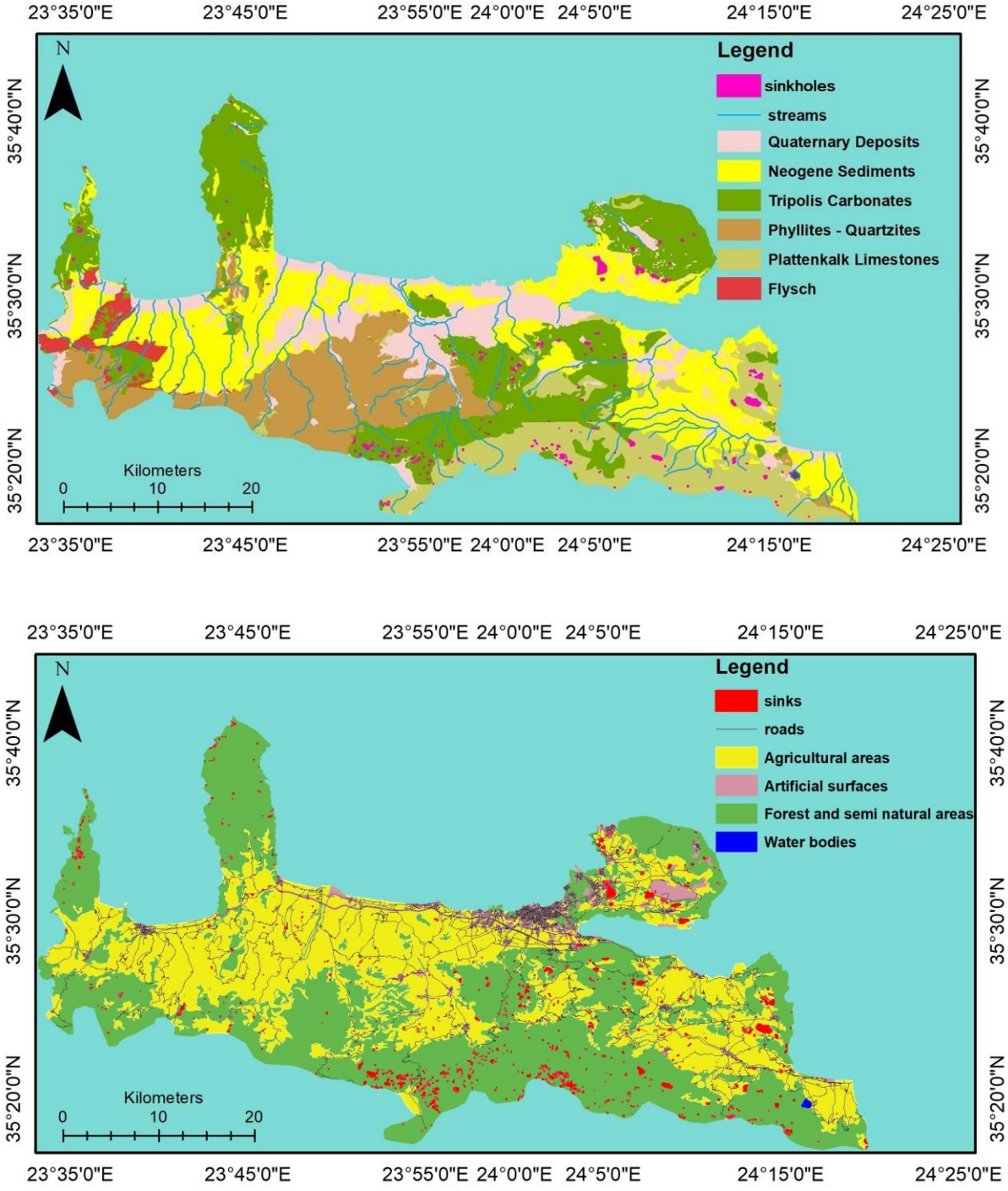

Fig.5: *(top) Geology map of the area with stream network on it and the final sinkholes of the 30-meter TanDEM-X DEM & (bottom) Land Use map of the area with faults and street network on it and the final sinkholes of the 11-meter TanDEM-X DEM*

2.2. Data selection & TanDEM-X description

2.2.1. Data selection

Two TanDEM-X DEMs of different horizontal resolutions (11m & 30m) were obtained by the TanDEM-X science service system (https://tandemx-science.dlr.de/). Geological and hydrology maps were digitized at a scale of 1:50,000, of the Greek Institute of Geology and Mineral Exploration. Groundwater exploitation, soil depth, faults, wells and drillings vector files were adapted by the Decentralized Administration of Crete (http://www.apdkritis.gr). Roads were downloaded by the Open Street Map (https://www.openstreetmap.org) and land use from CORINE European Environment Agency (EEA) inventory (http://www.eea.europa.eu). For a better validation of the sinkholes while applying the filter mechanisms and for adding other sinkholes that were not identified by the DEMs I used historical Google Earth imagery.

Table 1: *The total files that were used in all methodology and their sources*

Files that we used in both stages	Source
Tan-DEM-X 11m & 30m	TanDEM-X Science server https://tandemx-science.dlr.de/
Roads	Open street map https://www.openstreetmap.org/
Land-use	European Environment Agency http://www.eea.europa.eu
Geology (Lithology)	Digitizing the geological maps, at a scale of 1:50,000, of the Greek Institute of Geology and Mineral Exploration
Hydrogeology	Digitizing the geological maps, at a scale of 1:50,000, of the Greek Institute of Geology and Mineral Exploration
Soil Depth	Decentralized Administration of Crete www.apdkritis.gr
Groundwater Exploitation	Decentralized Administration of Crete www.apdkritis.gr
Streams	Extracted from TanDEM-X 30m
Faults	Digitizing the geological maps, at a scale of 1:50,000, of the Greek Institute of Geology and Mineral Exploration
Deep wells	Decentralized Administration of Crete

	www.apdkritis.gr
Slope	Extracted from TanDEM-X 11m
Elevation	Extracted from TanDEM-X 11m
Quarries	Decentralized Administration of Crete www.apdkritis.gr

2.2.2. TanDEM-X and DEM products

It was first launch in June 2010 by DLR (German Aerospace Center), along with EADS Astrium GmbH & Infoterra GmbH partners. TanDEM-X (TDX) satellite flies in a close formation with another, almost identical satellite, with the name TerraSAR-X (TSX) (fig.6). TanDEM-X is the first, single-pass, high-resolution multistatic SAR interferometer in space, which has as a primary objective to acquire a globally consistent and up-to-date Digital Elevation Model (DEM) with a unique accuracy" [42]. It actually corresponds to the model specifications of the High Resolution Terrain Elevation, level 3 (HRTE-3) which are; 12m posting & 2m relative height accuracy for flat terrain), while the absolute high accuracy is 1m.

TanDEM-X involves a unique data set to exhibit new bistatic and multistatic radar techniques for enhanced bio- and geophysical parameter retrieval [42]. The typical cross-track distances are 300m to 500m and so it has the ability to provide highly accurate velocity measurements of moving objects within a large coverage area. Both of the satellites contain a powerful modern radar system, the Synthetic Aperture Radar (SAR) system, which gives the opportunity to observe Earth's surface with or without solar light and in cloud conditions. TanDEM-X's sensitivity is able to adapt a broad spectrum of velocities ranging from less than a millimeter per second to more than hundred kilometers per hour [39]. Potential applications from comparing two or more single-pass (large baseline) cross-track TDX interferograms is the detection oftopographic changes that have occurred as a result of earthquakes or in the grounding line which separates the shelf from the inland ice in polar regions, agricultural areas or urban zones, monitoring of vegetation growth, mapping of atmospheric water vapor with high spatial resolution, measurement of snow accumulation or the detection of anthropogenic changes of the environment, e.g. due to deforestation. Another advantage of the combination of TDX/TSX is that they capture Earth with uniform accuracy and the DEMs have no gaps.

Across-track SAR interferometry techniques [43]:

• Topography: Adaption of a high resolution DEM with global access for topographic mapping.

• Navigation: There is a strong need of a worldwide precise and reliable terrain data base.

• Glaciology: Accurate maps of surface topography are a key pre-condition for monitoring and modeling glacier mass balance, glacier climate interactions and run-off from glacier basins.

• Hydrology: High spatial resolution DEMs for regional flood plain mapping.

• Oceanography: High spatial resolution for the estimation of two-dimensional ocean wave spectra and the determination of wind fields.

• Geology: Provides DEMs of high spatial resolution for geo-hazard mapping.

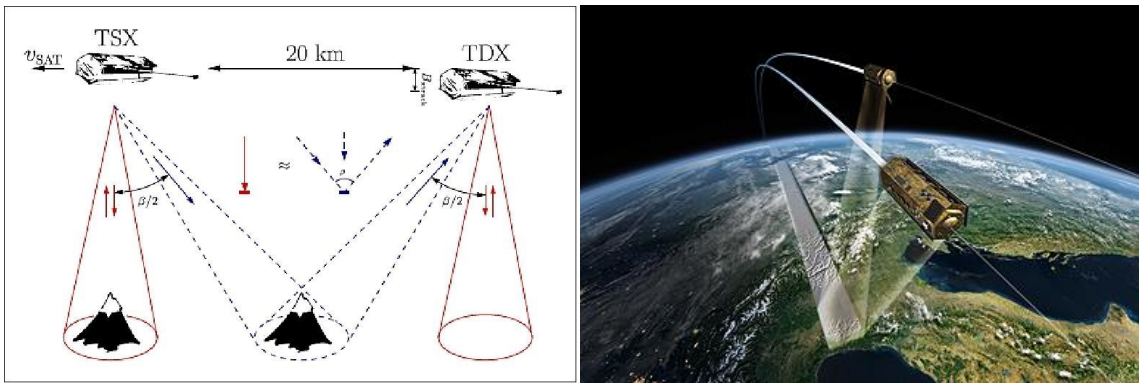

Fig 6: *The footage and distances of the two satellites TanDEM-X and TerraSAR-X flying together (https://www.dlr.de/rd/en/desktopdefault.aspx/tabid-5163/8674_read-17828/8674_page-3/gallery-1/216_read-3/)*

Slight changes in the soil and vegetation structure reflecting vegetation growth and loss, freezing and thawing, fire destruction, human activities, and so on can be obtained by TanDEM-X DEMs.

Chapter 3 Methodology

This study consists of two parts.

The first is to identify and map the sinkholes in the study area using two TanDEM-X DEMs with different horizontal resolutions; one of 11m and one of 30m.After sinkholes mapping in the study area and due to DEM resolution limitations and to offset inherent errors in DEM datasets, filter mechanisms and validation measures should be applied in order to improve their accuracy.

The second part is the generation of a sinkhole susceptibility map, in order to define which areas are vulnerable to sinkhole formation. The chosen method for this part of the study was the Frequency Ratio method.

3.1. Sinkhole formation mapping

This sinkhole mapping methodology adapted from [58] [45], [46] and [47] to produce sinkhole inventories of which sinkhole density measurements were derived. For the sinkhole formation mapping two TanDEM-X images were used separately, one with a spatial resolution of 11m and one of 30m respectively.

Same procedure was followed for both DEMs separately for sinkhole creation mapping (flow chart 1).

The two DEMs were at first clipped in the desired area and they were filled to their spill level. The initial DEMs were then subtracted from the filled ones and the differenced data effectively identified each depression in the original DEM and provided geometric characteristics [46]. The depressions were then converted to polygons, where 1038features were identified for the 11-meterTanDEM-Xand 428 for the 30-meterTanDEM-X. Filter mechanisms should be applied to exclude possible falsely identified sinkholes. These artificial sinkholes might be a result of misinterpretation of shallow or intermittent stream channel features, road construction [45], swimming pools, quarries etc. Vector files of street network, streams and quarries coupled with the inventory map were integrated in a GIS environment for the filter mechanisms. The chosen geometric characteristics were depth, eccentricity, circularity index (CI) and area. They were calculated and attributed to each sinkhole polygon in order to improve the accuracy of the identified

true sinkholes [48][49]. For the filtering “proximity to road” and ”proximity to stream” a checking through Google Earth imagery was proved useful, so there would not be falsely removed any known sinkholes. A final checking through Google Earth imagery took place after applying all the filter mechanisms in order to enriched our sinkhole inventory with unidentified by TanDEM-X sinkholes.
A description of the filters is following bellow the flow chart.

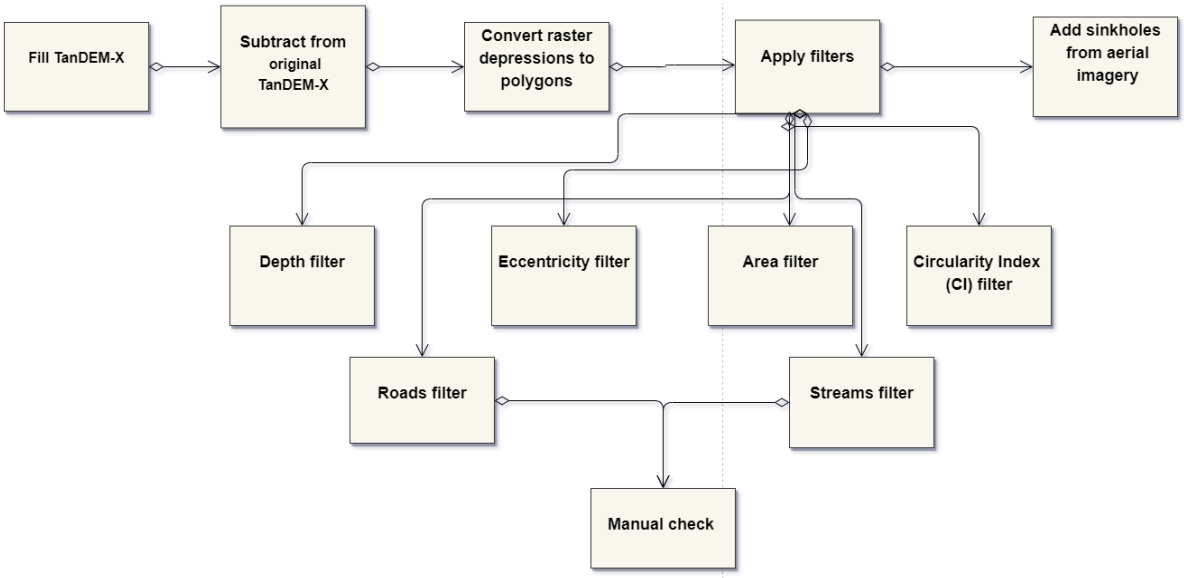

Flow chart 1: *The procedure that were followed for sinkhole formation mapping*

3.1.1. Area filter

The first filter is about sinkholes area and it refers to the boundary of each sink defined by the elevation of the spillover point [49]. Artificial sinkholes could be appeared as a result of horizontal accuracy errors, thus a chosen area threshold was applied. For 11-meter DEM the threshold was 244m^2 and for the 30-meter DEM 1800m^2.

3.1.2. Depth filter

It refers to the difference between bottom elevation and spill over elevation within each sinkhole [49]. Depth filter was based on the vertical accuracies of the TanDEM-X, which are 2.88m root-mean-square error (RMSE) for both TanDEM-X images. The range value between bottom elevation and spill over elevation was used for depth’s determination from the differenced raster.

3.1.3. Eccentricity filter

Eccentricity is a measure of how much a sinkhole deviates from being circular. It ranges between 0 and 1. Zero represents a perfect circle, while one represents a completely elongated ellipse a line. According to [47], sinkholes with eccentricity higher than 0.96 were excluded from the inventory map.

$$\boldsymbol{e = \sqrt{1 - \frac{b^2}{a^2}},}$$

Where, a and b are one-half of the depression's major and minor axes, respectively [47].

3.1.4. Circularity Index (CI) filter

Given the sinks known area, what would the perimeter be if it were a perfect circle, then compare it to its actual perimeter [46].

$$CI = \frac{Area}{3.14 * (2 * \frac{Area}{Perimeter})^2}$$

According to Douglas Ade [49] sinkholes with a CI less than 1.7 were removed from the inventory map.

3.1.5. Proximity to roads filter

Identified sinkholes at a distance of 4m from either side of the central road line were removed to eliminate falsely identified sinkholes in constructed road ditches (such as manholes, bridges, crossing roads etc.). Only the sinkholes that had up to the 50% of their area in the buffer distance were removed from the inventory map based on [47]. The 4-meter distance was determined by checking Google Earth high-resolution aerial imagery.

3.1.6. Proximity to streams filter

As in roads filter mechanism, identified sinkholes at a distance of 31m from either side of the central stream line were removed to eliminate falsely identified sinkholes by stream-depressions that are created mostly due to erosion by rainfall. Once more the distance was determined through Google Earth's high-resolution aerial imagery, but at this time all the sinkholes that existed at this distance from the central stream

line were removed, except from 5 sinkholes that were already known and were kept manually.

Table 2: *The parameters that were calculated for the sinkhole formation inventory map along with the calculation method and each parameter's threshold.*

Parameters	Calculation Method	Threshold
Depth (m) [1], [34]	Zonal Statistics as a Table (range)	>2.88m
Major / Minor Axes (m) [47], [49]	Zonal Geometry as a Table	
Eccentricity [47], [49]	Select by attributes; $\sqrt{1-\frac{(Minor\ Axes/2)^2}{(Minor\ Axes/2^2}}$	<0.96
Perimeter (m)	Zonal Geometry as a Table	
Area (m²) [47]	Zonal Geometry as a Table	>3 pixels
Circularity Index [49]	Select by attributes; $CI = \frac{Area}{3.14(2 * \frac{Area}{Perimeter})^2}$	<1.7
Volume (m³) [49]	Zonal Statistics as a Table (Sum * pixel value)	
Roads [47]	Select by location (have their center in)	4m
Streams [47]	Select by location (within a distance)	31m

Table 3: *Number of sinkholes after each filter mechanism*

Sinkholes	TanDEM-X11	TanDEM-X30
initial	82,897	14,242
area	40,830	57,04
eccentricity	36,839	50,53
Circularity Index	1,1505	1,115
depth	2,218	487
roads	2,154	481
streams	1,038	428

3.2. Frequency Ratio Method

In this study Frequency ratio technique coupled with a detailed sinkhole inventory through the use of **TanDEM-X,** has been chosen to produce a sinkhole susceptibility map. This method is being used for two reasons; (a) in order to make a statistical approach of simulation environmental conditions and (b) to link the related factors to the dependent factor. When evaluating the probability of sinkhole formation within a specific period of time and a certain location, it is very important to determine the conditions under which sinkholes are formed and the factors that could trigger such events (such as mining exploitation or rainfalls). It belongs to statistical methods and thus it is more applicable for prediction and classification of environmental problems in various regions. In frequency ratio method the ratio is that of the sinkholes area, to the total area, so that a value of 1 is an average value. If the value is greater than 1, it means that the percentage of the sinkhole is greater than the area and so there is a stronger correlation. If the value is lower than 1 then the opposite applies and the correlation is low.

$$FR = \frac{A/B}{C/D}$$

Where, A is the area of a class for the factor, B is the total area of the factor, C is the number of pixels in the class area of the factor, D is the total number of pixels in the

study area, ***A/B*** is the percentage of total area and ***C/D*** is the percentage of sinkhole area.

As it is has been mentioned, the geological characteristics of the study area are very important factors in sinkhole formation and thus are important of susceptibility analyses. Such characteristics are the geologies of the area, the hydrogeology, the faults, the slope, the aspect, the elevation and the depth of soil. Other important factors are the land use, the present of mines and of deep wells, the streams, the groundwater fluctuations, the groundwater exploitation and the vegetation of the area and some chemical and physical characteristics of groundwater (pH, alkalinity, K+, Ca+ etc).

3.2.1. Prediction Analysis – Sinkhole Susceptibility method

The second part of the study starts with the preparation of a sinkhole inventory map based on satellite images, DEM images and existed bibliography. In order make the prediction analysis and prepare the sinkhole susceptibility map quantitatively, the frequency ratio model was applied in GIS. Using this model it is possible to derive the spatial associations of sinkhole's location compared with each of the contributed factors in sinkhole occurrence. This model is based on the analysis of the relation between sinkholes and the attributed factors [41]. The chosen 12 possible factors and the sources that were acquired are presented in table 4. A sinkhole susceptibility map provides the spatial distribution of the existing sinkholes that were determined by the sinkhole formation mapping at the first part of the Thesis. For the preparation of the inventory map the 70% (727) of the total (1038) sinkholes of the 11-meter spatial resolution TanDEM-X map was used as a training dataset and the other 30% (311) was used as the test dataset.

The three steps that were followed for the generation of the sinkhole susceptibility index were the followed [50];

1. Determine rates for each class of the twelve factors based on the frequency-ratio statistical method;
2. Generate individual susceptibility maps for each factor based on literature and frequency-ratio statistical method;

3. Calculate the sinkhole susceptibility index as a sum of the individual susceptibility maps.

Table 4: *Factors related to sinkhole formation and the calculation method*

Factors related to sinkhole formation	Calculation method
Slope [8]	Slope tool, by TanDEM-X 11m
Elevation [47], [8]	Categorized of the TanDEM-X 11m values
Land-use [47], [8]	Classification of the different types
Geology (Lithology) [64], [8]	Classification of the different types
Hydrogeology	Classification of the different types
Soil Depth [47], [8]	Classification of the different types
Groundwater Exploitation [47]. [8]	Interpolation analysis
Distance to faults [8]	Euclidian distance
Density of faults [8]	Kernel density
Density of deep wells [8]	Kernel density
Drainage density [8]	Kernel density
Distance to deep wells	Euclidian distance

3.2.1. Geology (Lithology)map

Lithology is one of the most important parameters since sinkhole formation is related to karst basins characteristics and thus it occurs in karst regions (both surface and subsurface formations). The reasons for not excluding from the beginning the non-karst regions are; (i) due to possible karst geology under bedrock and (ii) to investigate probable spatial relations of sinkhole occurrence and the different geological formations. Six classes were generated, as much as the different types of geological formations in the study area; (i) Quaternary Deposits, (ii) Neogene Deposits, (iii) Tripolis Carbonates, (iv) Phyllites – Quartzites, (v) Platenkalk Limestones and (vi) Flysch (fig.7).

3.2.2 Drainage density map

Drainage density refers to the total length (m) of drainage line per unit area (km^2) [54]. The map was calculated with Kernel density and it was classified into 5 classes using the Natural Breaks classification method; (i) 0 –0.10(km/km^2), (ii) 0.10 – 0.29(km/km^2), (iii) 0.29 – 0.49(km/km^2), (iii) 0.49 – 0.77(km/km^2) and (v) 0.77 – 1.45(km/km^2) (fig.7).

3.2.3 Distance to deep wells map

In many cases it has been noticed that the existence of deep wells in karst aquifers activates sinkhole formation. 237 digitized deep wells were downloaded from the Decentralized Administration of Crete in order to calculate the proximity map and then to classify it into 5 categories; (i) 0–250m, (ii) 250–500m, (iii) 500–1000m, (iv) 1000–2000m and (v) < 2000m (fig.8).

3.2.4. Distance to faults map

Based on previous studies, a correlation of sinkhole formation and proximity to existing fault lines exists, because of the fact that faults provide a quick route for groundwater to percolate into [52]. This map was created with the calculation of Euclidian distance and was classified in five categories from the faults based on literature and adapted to the limitations of the study area. The five classes are the followed; (i) 0–200m, (ii) 200–500m, (iii) 500–1000m, (iv) 1000–1500mand (v) >1500m (fig.8).

3.2.5. Density of deep wells map

The map was calculated with Kernel density and it was classified into 5 classes using the Natural Breaks classification method; (i) 0 – 0.169(km/km^2, (ii) 0.169 - 0.54(km/km^2), (iii) 0.54–0.96(km/km^2), (iv) 0.96 – 1.49(km/km^2) and (v) 1.49 – 3.07(km/km^2)(fig.9)

3.2.6. Elevation

Elevation seems to be an important criterion as well, especially on hilly areas [51] [8]. Sinkhole formation is expected to be seen in high altitudes. According to the limitations and the characteristics of our study area, nine classes of elevation were categorized from TanDEM-X 11m, with an interval of 250m; (i) 0-250, (ii) 250-500, (iii) 500-750, (iv) 750-1000, (v) 1000 – 1250, (vi) 1250-1500, (vii) 1500-1750, (viii) 1750-2000, (ix) >2000 (fig.9).

3.2.7. Groundwater exploitation map

Groundwater exploitation refers to the rate of groundwater pumping from wells in Mm^3 per year and it shows the distribution of groundwater retreat points and their relative importance [51]. Both the vector file and the values of annual

pumping were downloaded by the Decentralized Administration of Crete, including records for over 500locations. The map was then created with interpolation analysis and it was categorized in 4 classes; (i) 0–100,000Mm^3, (ii) 100,000– 400,000Mm^3, (iii) 4,600,000 – 1,800,000Mm^3 and (iv) 1,800,000 - 4,900,000Mm^3 (fig.10).

3.2.8. Density of faults map

Fault density refers to the cumulative length of faults (m) per unit area (km^2) [53]. A high density of faults in carbonate bedrock might increase the permeability of the ground, having as a result the circulation of groundwater, the formation of structurally-controlled cavities and the occurrence of sinkholes [5]. The fault density was calculated by using Kernel density and was grouped into 5 classes using the Natural Breaks classification method; (i) 0–0.169(km/km^2), (ii) 0.167–0.54(km/km^2), (iii) 0.54–0.96(m/km^2), (iv) 0.96–1.47(km/km^2) and (v) 1.47–3.07(km/km^2)(fig.10).

3.2.9. Hydrogeology map

Hydrogeology map provides the information of the permeability of the rocks. Based on literature rocks with high permeability are prone to sinkhole formation. Karst environments are characterized from high permeability. The map was classified in 8 categories; (i) medium to low permeability rocks, (ii) high permeability rocks, (iii) low permeability rocks, (iv) medium permeability rocks, (v) high Miocene permeability rocks, (vi) medium Miocene permeability rocks, (vii) impervious rocks and (viii) non-permeability rocks (fig.11).

3.2.10. Land Use map

Urban areas or areas with limited / low vegetation are expected to be vulnerable to sinkhole formation. In the study area, the CORINE Land Cover - Land Use map 2000, was obtained from http://www.eea.europa.eu and four classes are used; (i) agricultural areas, (ii) artificial areas, (iii) forest & semi-natural areas and (iv) water bodies (fig.11).

3.2.11. Soil Depth map

The thicker the soil is, the greater the size of the cavity that may form within it and collapse [26]. Soil depth dataset was downloaded from the Decentralized Administration of Crete and it was classified in the following ten categories; (i) unspecified, (ii) bare, (iii) bare &deep, (iv) bare & shallow, (v) deep, (vi) deep & bare, (vii) deep & shallow, (viii) shallow, (ix) shallow & bare and (x) shallow & deep (fig.12).

3.2.12. Drainage density map

The slope map produced from the TanDem-X with a spatial resolution of 11.1 meters was further classified into five classes according to [37]; (i) 0-5 degrees, (ii) 5-15 degrees, (iii) 15-30 degrees, (iv) 30-45 degrees and (v) <45 degrees (fig.12).

Table 5: *Frequency–ratio values and class rates for each of the twelve controlling factors.*

Controlling factors	classes	% of total area (a)	% of sinkhole area (b)	Frequency Ratio (b/a)
Slope (degrees)	0 – 5	17.59	34.41	1.96
	5 – 15	31.17	38.56	1.24
	15 – 30	36.41	21.26	0.58
	30 – 45	13.29	3.56	0.27
	< 45	1.53	2,.99	1.43
Elevation (m)	0 – 250	46.52	27.83	0.60
	250 – 500	25.78	31.48	1.22
	500 – 750	13.50	13.87	1.03
	750 – 1,000	4.85	1.99	0.41
	1,000 – 1,250	3.75	11.20	2.98
	1250 – 1,500	2.62	4.02	1.53
	1,500 – 1,750	1.68	2.29	1.36
	1,750 – 2,000	1.08	6.87	6.36
	< 2,000	0.20	0.44	2.19
Soil Depth	Unspecified	0.45	0	0
	Bare	1.22	7.55	6.16
	Bare & Deep	5.97	3.33	0.56
	Bare & Shallow	14.99	17.07	1.14
	Deep	21.89	8.09	0.37

	Deep & Bare	3.57	21.32	5.98
	Deep & Shallow	24.00	6.56	0.27
	Shallow	1.83	0.15	0.08
	Shallow & Bare	15.78	25.01	1.58
	Shallow & Deep	10.31	10.92	1.06
Land Use	Agricultural areas	44.61	45.57	1.02
	Artificial areas	3.06	1,70	0.56
	Forest & semi-natural areas	52.29	52.73	1.01
	Water bodies	0.62	0	0
Hydrogeology	High permeability rocks	5.84	4.87	0.83
	Medium to low permeability rocks	32.37	48.07	1.48
	High permeability rocks	16.59	5.19	0.31
	Low permeability rocks	10.86	27.75	2.55
	Medium permeability rocks	1.07	0.90	0.84
	High Miocene permeability rocks	14.00	9.95	0.71
	Medium Miocene permeability	17.80	3.15	0.18
	rocks	1.48	0.13	0.08
	Impervious rocks			
	Non-permeability rocks			
Groundwater	0 – 100,000	69.30	58.66	0.85
Exploitation	100,000 – 400,000	28,58	38.63	1.35
(Mm³/year)	400,000 – 1,800,000	1,68	2.47	1.47
	<1,800,000	0,43	0.23	0.53
Distance to	0 – 250	2.92	2.75	0.94
deep wells	250 – 500	6.57	4.09	0.62
(m)	500 – 1,000	15.94	7.33	0.46
	1,000 – 2,000	26.72	11.78	0.44
	< 2,000	47.85	74.04	1.55
Distance of	0 – 200	30.50	34.16	1.12
faults (m)	200 – 500	29.63	29.05	0.98
	500 – 1,000	24.02	29.70	1.24
	1,000 – 1,500	9.16	6.01	0.66
	<1,500	6.68	1.071	0.16
Deep wells	0 – 0.17	7.95	0.78	1.61
density	0.17 - 0.54	18.37	9.05	0.91
(km/km²)	0.54 – 0.96	12.93	8.83	0.49
	0.96 – 1.49	23.44	21.36	0.68
	1.49 – 3.07	37.31	59.97	0.10
Faults	0 – 0.17	5.38	2.52	0.47
density	0.17– 0.54	23.29	18.41	0.79
(km/km²)	0.54– 0.96	34.55	42.77	1.24
	0.96 – 1.47	25.78	24.72	0.96

	1.47– 3.07	11.00	11.58	1.05
Drainage density (km/km²)	0 – 0.10	13.23	19.51	1.47
	0.10– 0.29	14.53	24.00	1.65
	0.29 – 0.49	22.031	18.53	0.84
	0.49 – 0.77	28.70	24.46	0.85
	0.77 – 1.45	21.51	13.49	0.63
Geology (lithology)	Quaternary Deposits	26.82	31.30	1.85
	Neogene Deposits	14.03	22.74	0.58
	Tripolis Carbonates	26.87	15.56	1.17
	Phyllites – Quartzites	15.00	27.82	0.16
	PlatenkalkLimestones	1.50	0.086	1.62
	Flysch	15.73	2.482	0.06

After calculating the frequency ratios, the sinkhole susceptibility index (SSI) was estimated for each pixel in the study area. The frequency ratio was calculated for sub-criteria of parameter and then the frequency ratios were summed to calculate the sinkholes susceptibility index.

$$SSI = Fr_1 + Fr_2 + Fr_3 + ... + Fr_{12}$$

where, Frequency-ratio is the rating of each factor's type or range [41]

Sinkhole Susceptibility Index is represented by a final map, where the vulnerable zones for sinkhole formation are observed. The map is classified in four classes of "Low", "Moderate", "High" and "Very High" susceptibility for sinkhole formation using the classification method of Equal Areas (fig.20). After the generation of Sinkhole Susceptibility Map, the test dataset of sinkholes is overlaid in order to evaluate the resulting map.

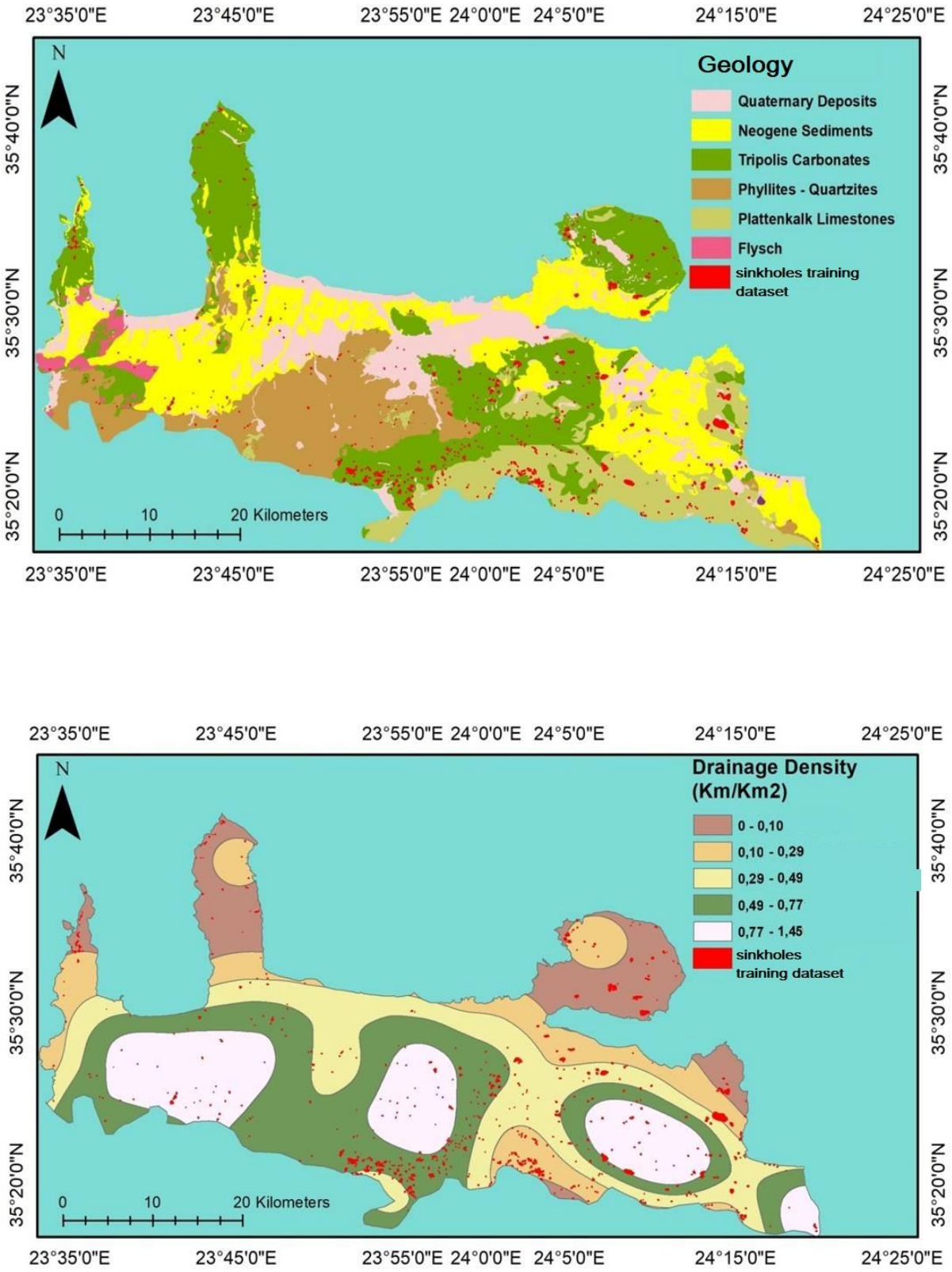

Fig.7: *Maps that show the classes of (top) geology (lithology) and (bottom) drainage density*

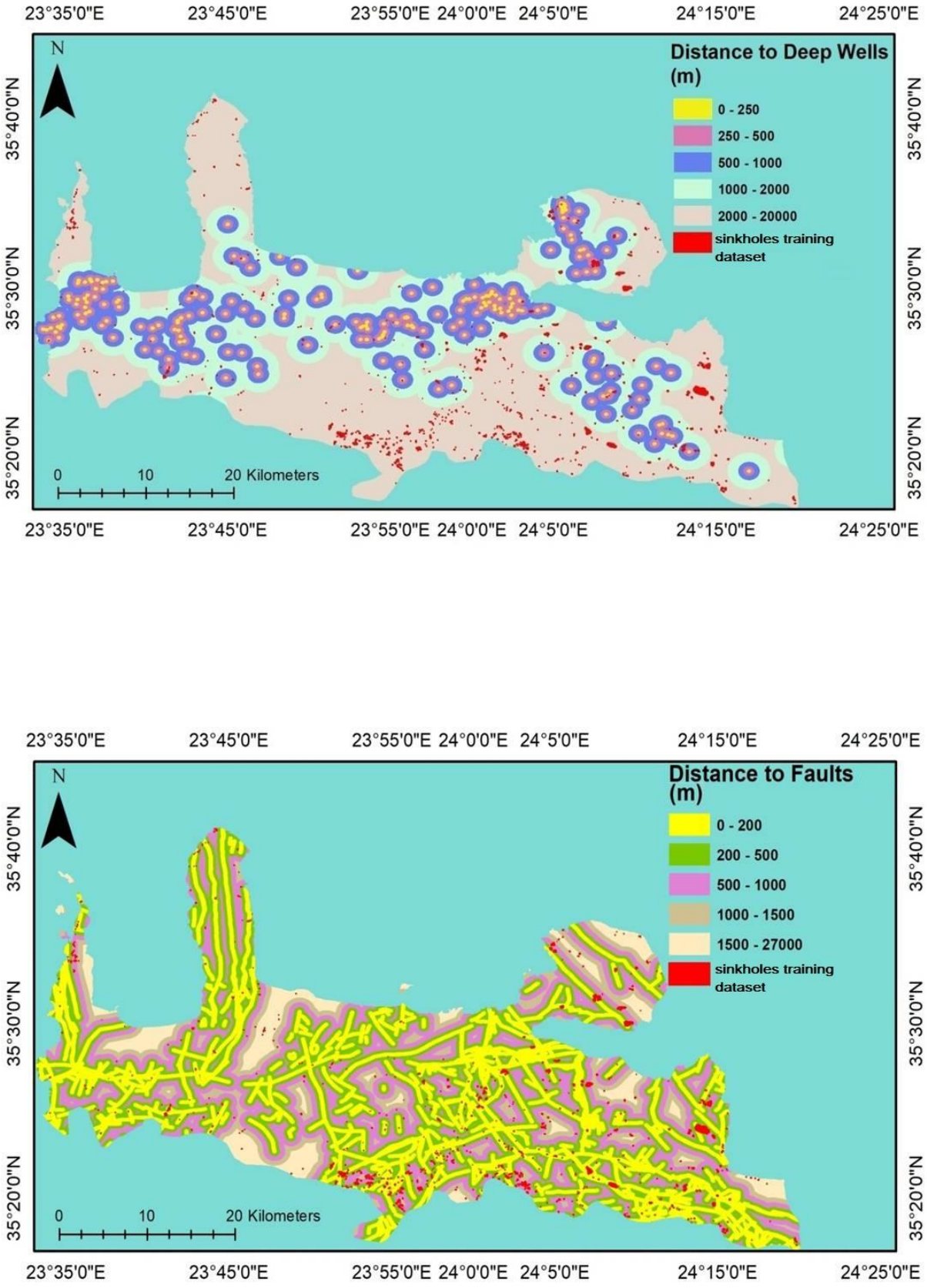

Fig.8: *Maps that show the classes of (top) distance to deep wells and (bottom) distance to faults*

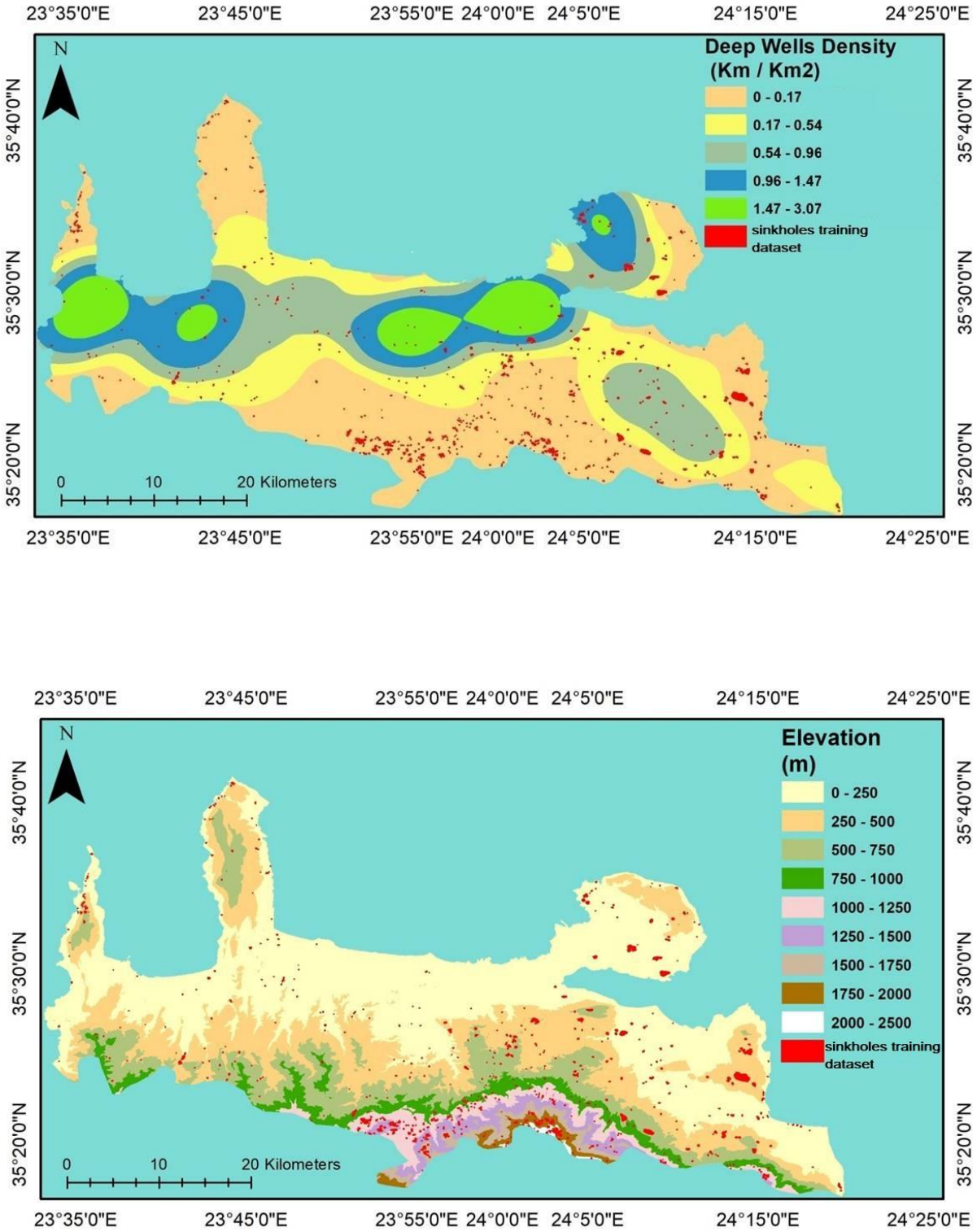

Fig.9: *Maps that show the classes of (top) density of deep wells and (bottom) elevation*

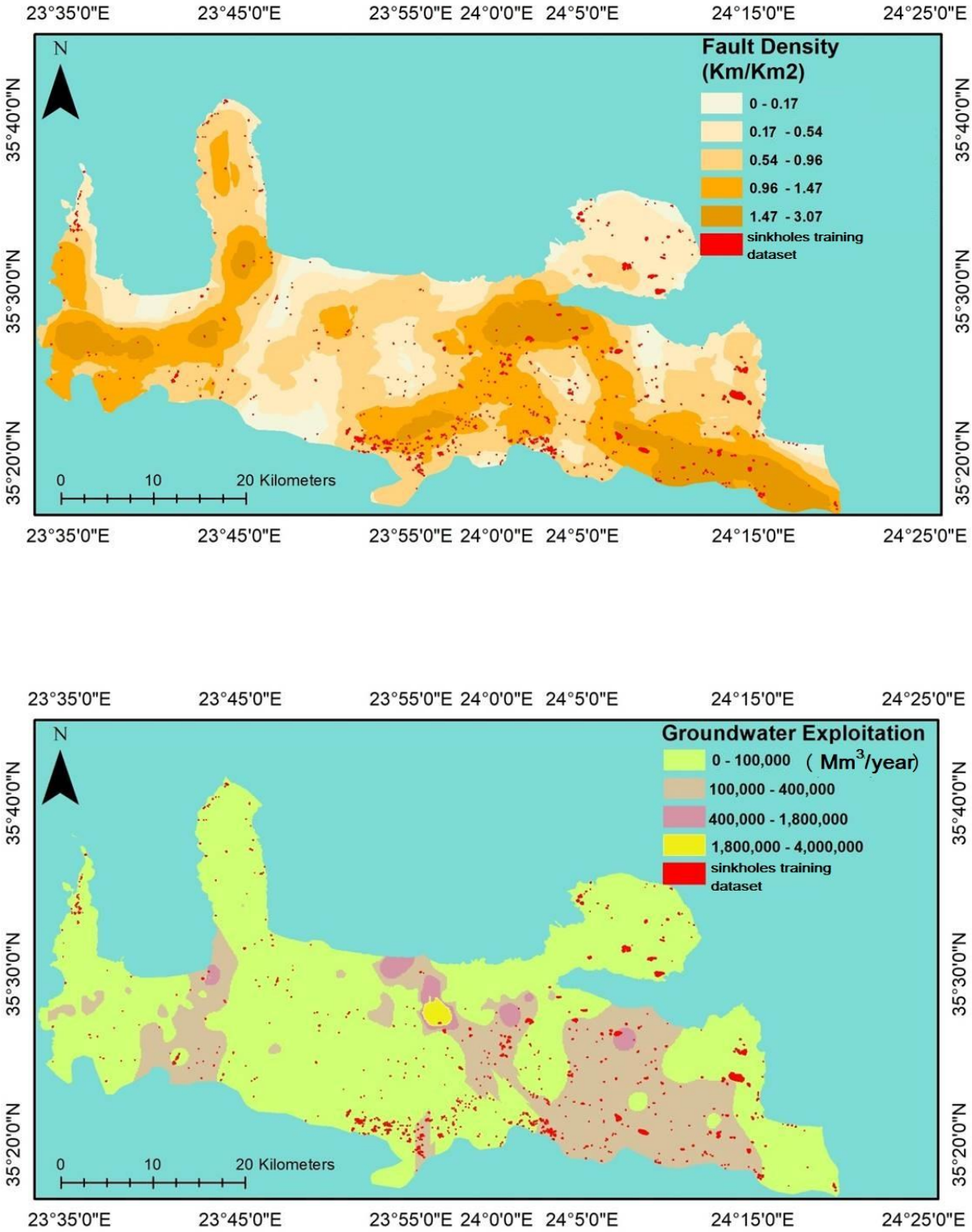

Fig.10: *Mapsthat show the classes of (top) fault density and (bottom) groundwater exploitation*

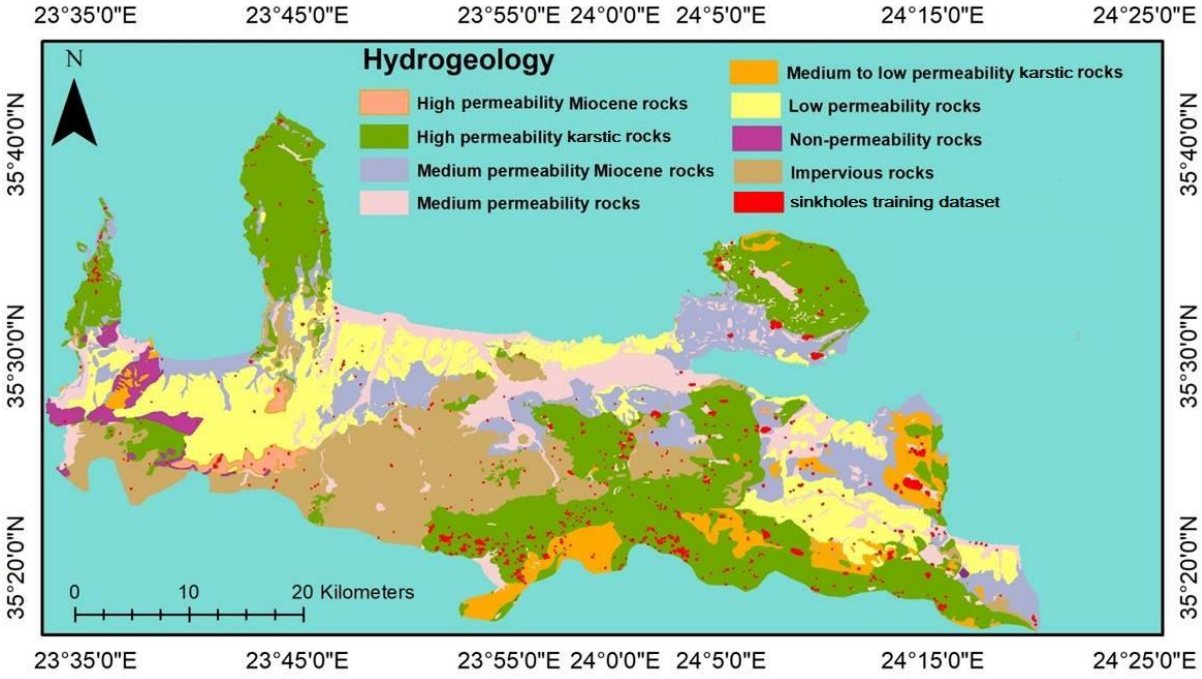

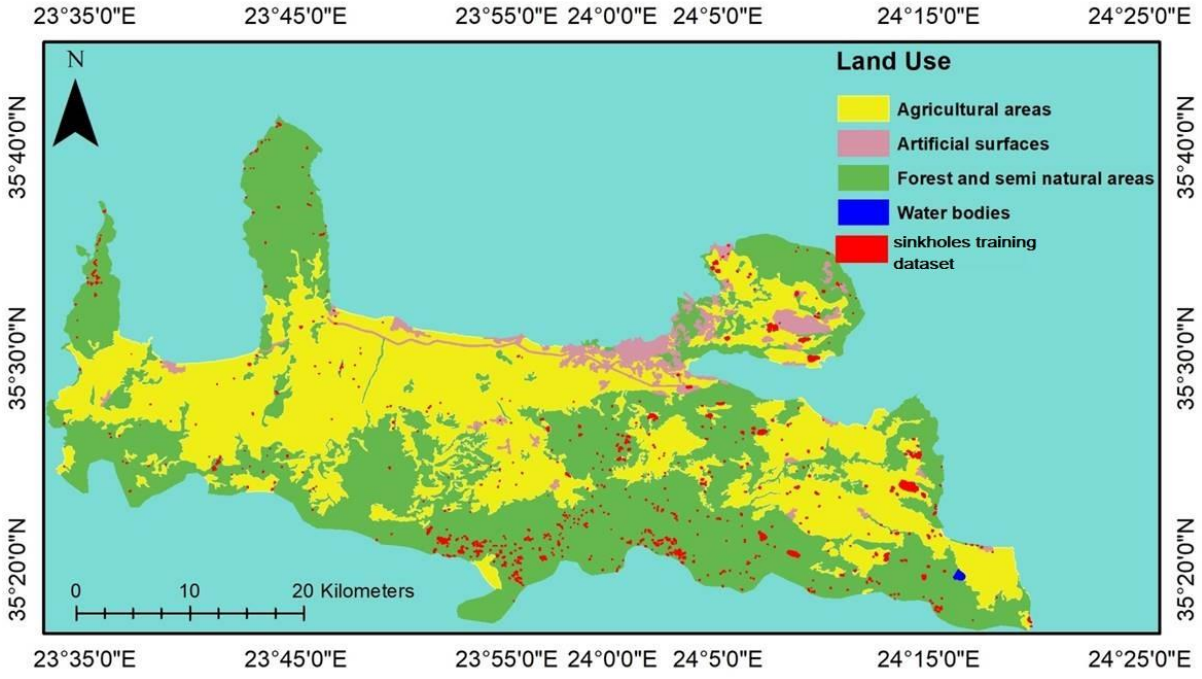

Fig. 11: Maps *that show the classes of (top) hydrogeology and (bottom) land use*

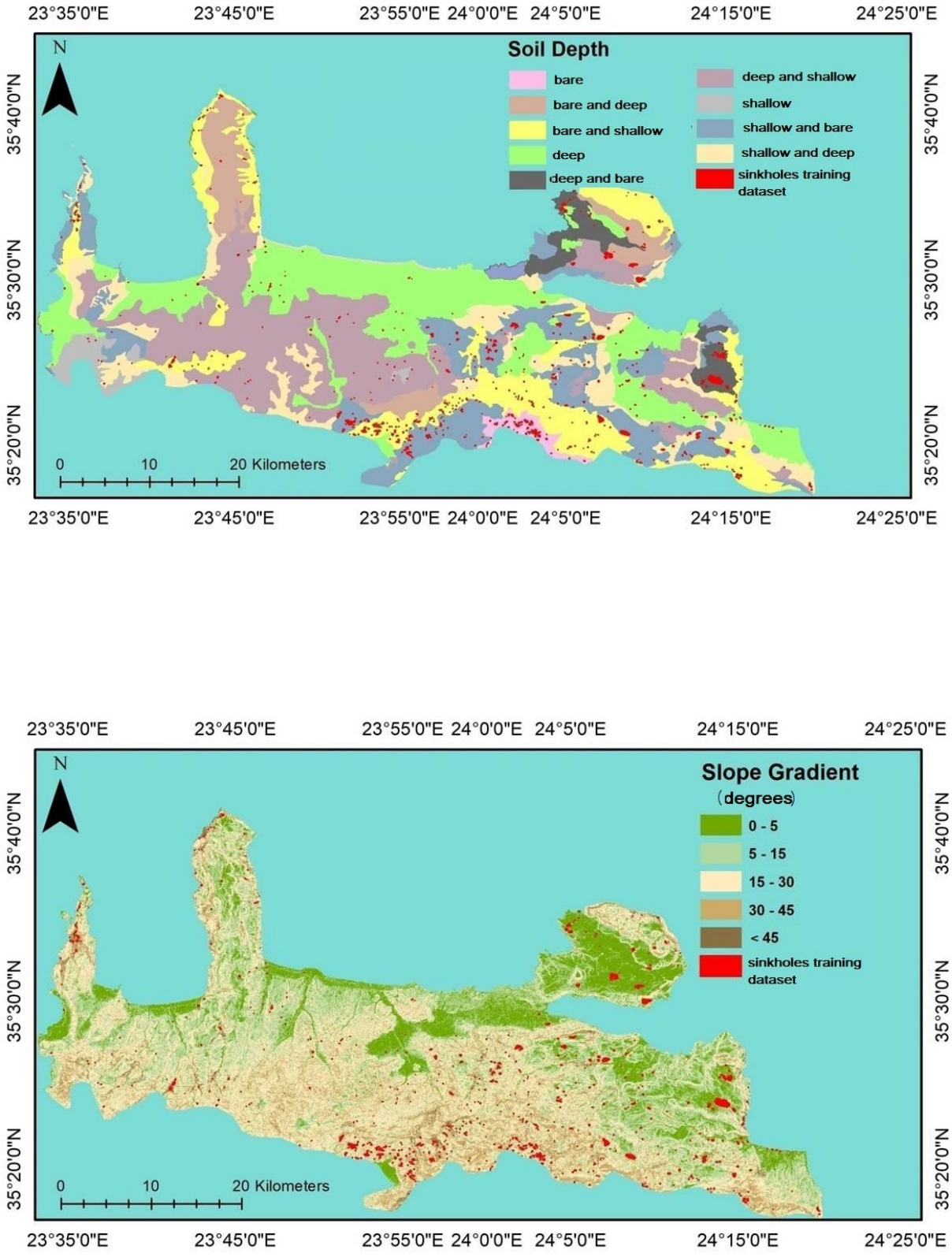

Fig.12: *Maps that show the classes of (top) soil depth and (bottom) slope gradient*

CHAPTER 4: RESULTS

Starting from the first part of this study, the 11-meter TanDEM-X digital elevation model has successfully recognized numerous sinkholes in the northern Chania area. The 30-meter TanDEM-X digital elevation model led to a smaller number of mapped sinkholes. This fact can be explained by the 11-meter TanDEM-X better spatial resolution and its ability to capture smaller sinkholes. In many cases the TanDEM-X of 30m spatially merged two or more sinkholes into one bigger (fig.13), which is again a result of the lower spatial resolution in comparison with the other DEM. The geometrical and statistical filters (area, eccentricity, circularity index and depth) excluded successfully over the 70% of the falsely-identified initial sinkholes without removing any of the known or real sinkholes. Based on ground-truthing, five existed sinkholes that were identified as artificial by the filters application (proximity of streams and roads) were not excluded from the final inventory map. Furthermore, some more unmapped sinkholes were added to the final dataset using the high resolution satellite image of Google Earth.

As for the prediction analysis, the chosen sinkhole inventory map was the one generated by the 11-meter TanDEM-X, due to the better spatial resolution and the bigger number of the in-situ verified sinkholes. The prediction analysis was held with the method of "frequency ratio", in which 12 susceptibility maps were generated, one for each factor, and then one final sinkhole susceptibility map was generated by the sum of the 12 weighed maps. The 70% of the total sinkholes were used as a training dataset and the rest 30% were used as the test dataset.

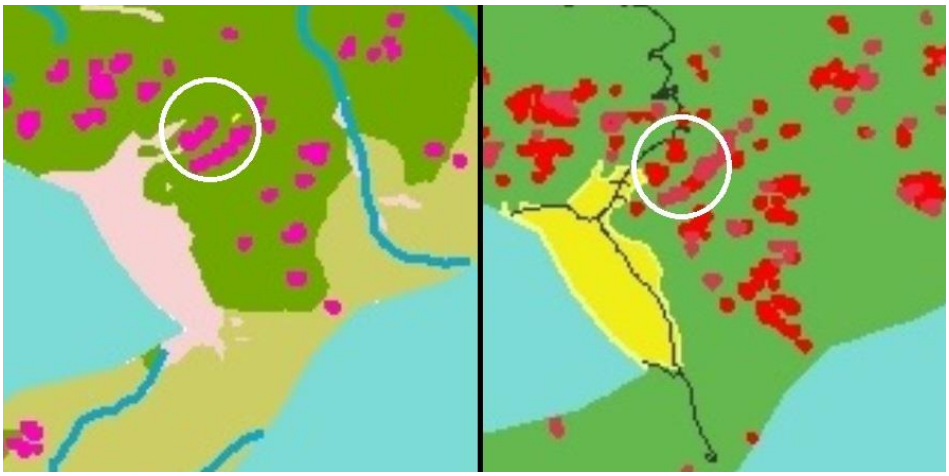

Fig.13: *Comparison of the spatial resolution in TanDEM-X 30m (left) and TanDEM-X 11m (right)*

It is of a great importance to discuss first the results of each factor susceptibility map, before the results of the final sinkhole susceptibility index.

According to susceptibility map of geology (fig.14), the training dataset shows high spatial correlation with the carbonate rocks. The highest ratios are observed in "Tripolis carbonates" and "Platenkalk limestones", which refer to karst terrains, as well as in "Quaternary deposits" which are known for being deposited on karsts. As it was expected, sinkhole formation in hydrogeology susceptibility map occurs in regions with rocks of medium and high permeability.

In soil depth susceptibility map (fig.19) the two highest ratios are observed at "bare" and "deep and bare" classes, which proofs that sinkhole formation is correlated with the absence of vegetation, especially in comparison with the presence of exposed limestones with deep soil. Since the soil depth is bigger, the groundwater fluctuations are greater.

A correlation in sinkhole creation and the existence of faults is being observed in both "faults' density" and "distance to faults" susceptibility maps (fig.15& fig.17). On distance to fault factor the range of affection is from 0m to 1000m and at faults' density is from 0.54(m/km^2) to 3.07(m/km^2) and especially from 1.47(m/km^2) to 3.07(m/km^2).

In "Land Use" susceptibility map (fig.18) the forest & semi-natural areas class shows almost equal rate with the agricultural areas and thus this factor will be consider as not important for this case. The two big available categories out of the four in total were similar and they should be classified into smaller and more detailed categories. It should be noticed here, that in the artificial class and especially in the city of Chania and along the coastline, a lot of false sinkholes were recognized by the DEM due to the existence of swimming pools and buildings and were removed.

Referring to slope map (fig.19), the higher frequency ratio is 0^o-5^o while high altitudes (more than 1,750m) (fig.16) shows the stronger spatial correlation with the mapped sinkholes. In lower elevations (750m -1,750m) the frequency ratio is also high, with the exception of elevated areas with steep slopes.

Sinkholes seem to preferably occur in distances greater than 2000m from the deep wells locations (fig.15). This observation can be explained by the fact that deep wells

in Chania area are preferably located mainly in agricultural areas. In bare terrains there is low to no activity and thus the existed data is limited to provide valid results. In the case of groundwater exploitation controlling factor, the frequency ratio is higher in greater densities (100000– 1800000(m/km^2).

Lastly, about "drainage density" susceptibility map (fig.14), the results give a high frequency ratio at the lowest densities classes (0.49(m/km^2) to 1.45(m/km^2)). It is known that at the karst regions of the study area the water flows mainly underground and thus there are no streams at these locations that could affect much the sinkhole creation.

The last part of this study was the prediction analysis by generating a sinkhole susceptibility inventory from the sum of the twelve susceptibility maps. In figure 20 the map is classified according to the equal areas method in four categories; (i) low, (ii) moderate, (iii) high and (iv) very high. On the map the polygons of sinkholes' test dataset are superimposed in order to evaluate the prediction analysis. A rate of 83.3% is formed on the "high" and "very high" classes, considering the prediction analysis as highly successful. Apart the high proportion of the successfully predicted sinkholes, it is well noted the fact that in many cases, (two of which are presented in figure 21), the shape of these depressions fits the borders between "very high" and "high" class.

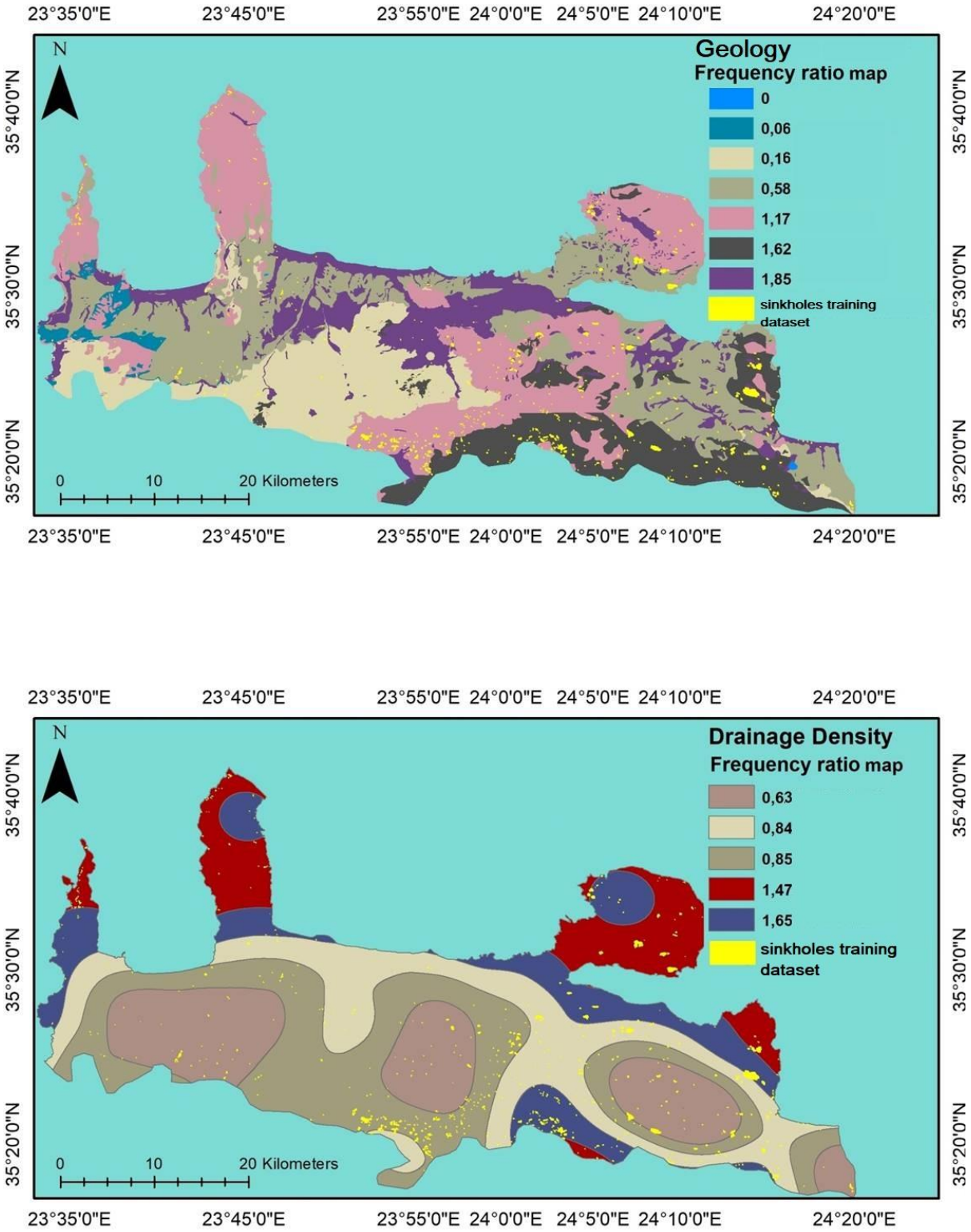

Fig.14: *Susceptibility maps of factors; geology (lithology) (top) and drainage density (bottom)*

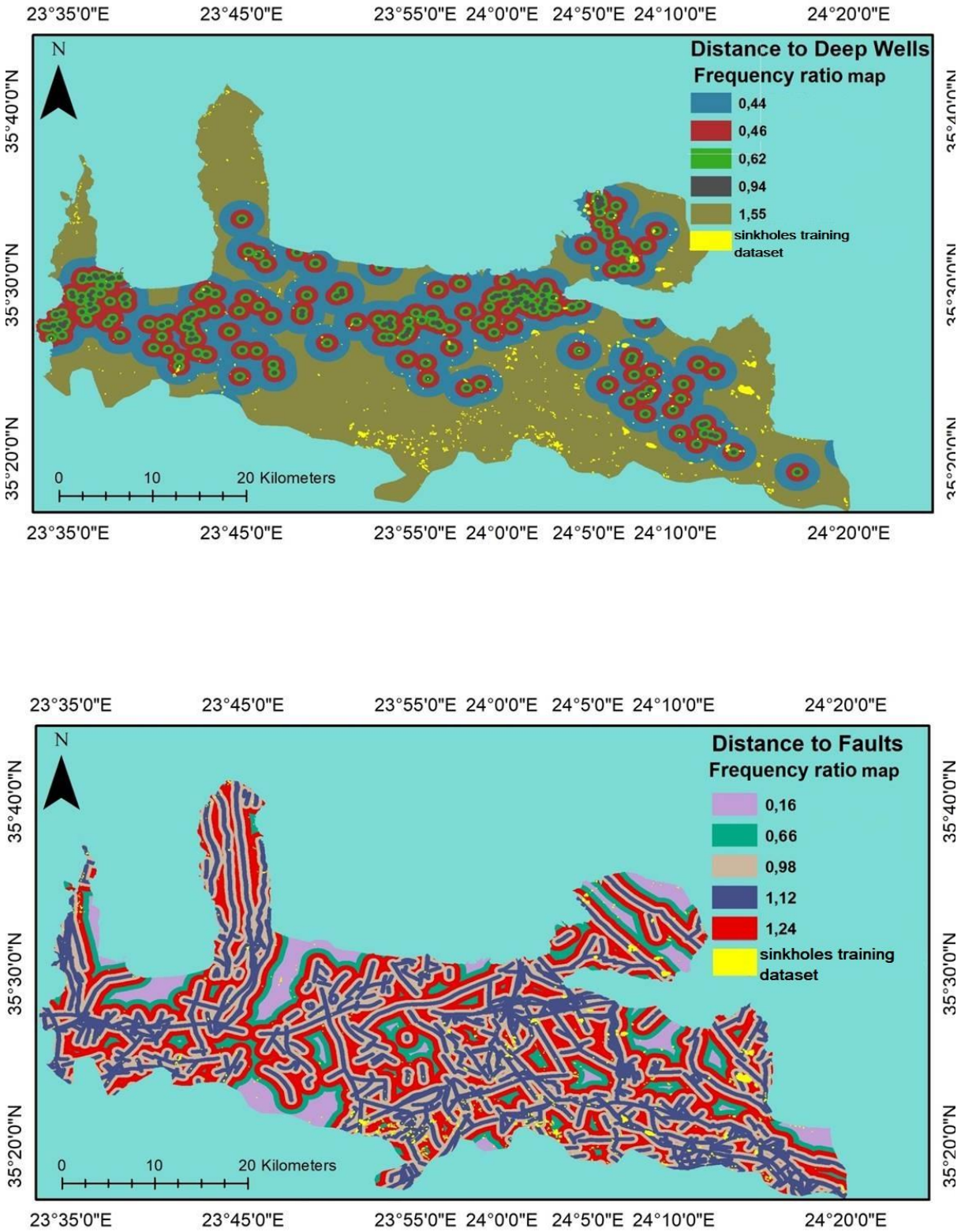

Fig.15: *Susceptibility maps of factors; distance to deep wells (top) and distance to faults (bottom)*

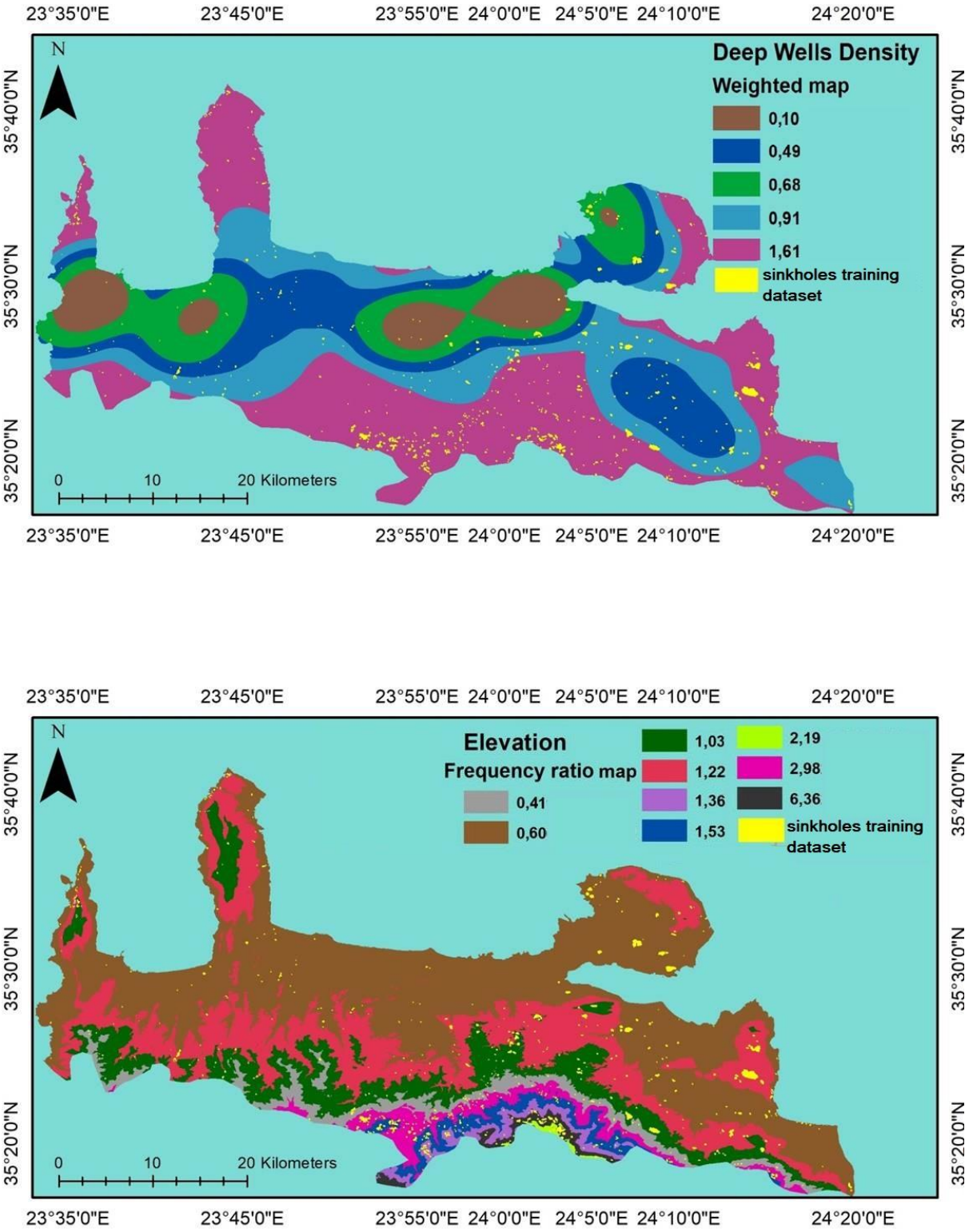

Fig.16: *Susceptibility maps of factors; deep wells' density (top) and elevation (bottom)*

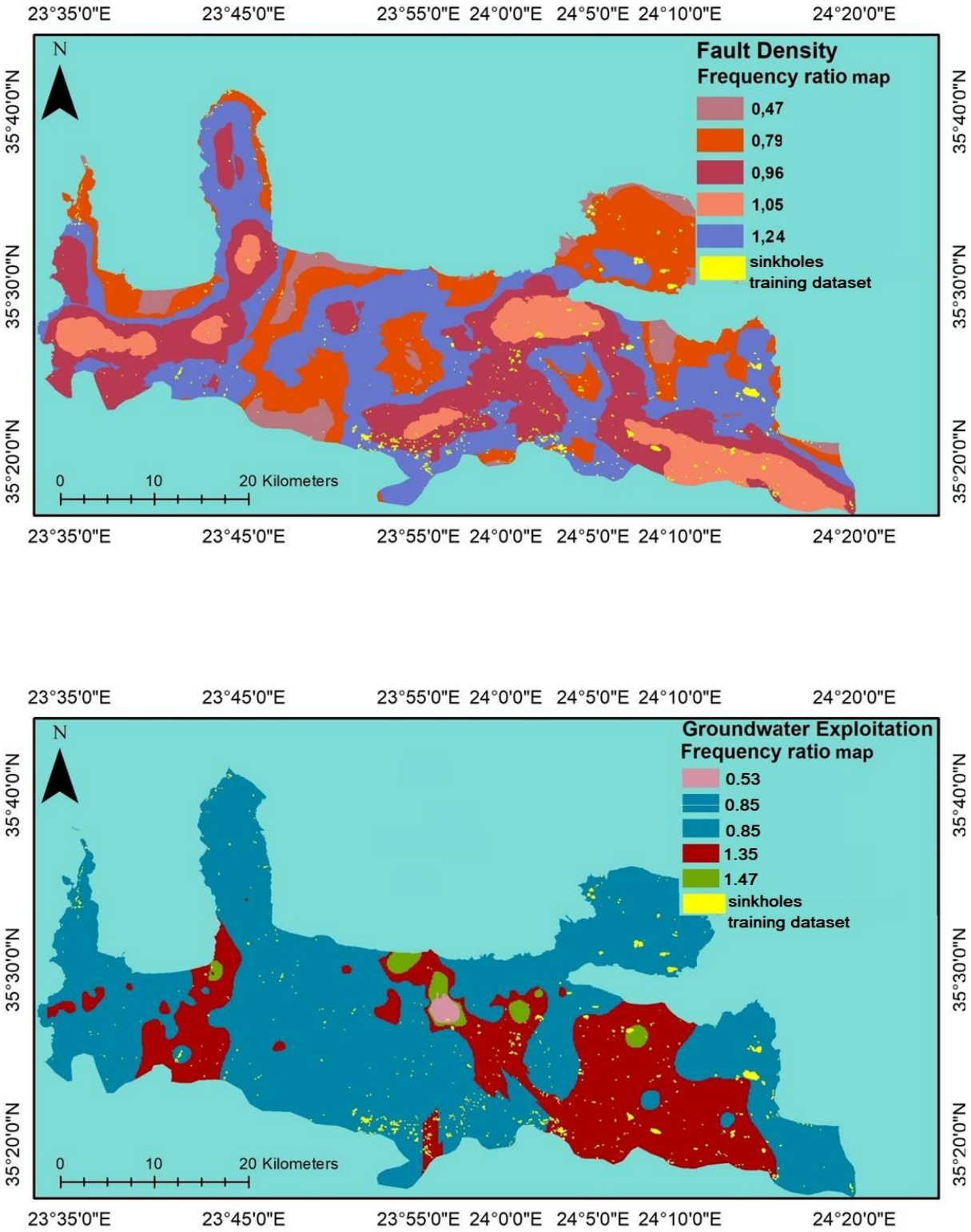

Fig.17: *Susceptibility maps of factors; faults' density (top) and groundwater exploitation (bottom)*

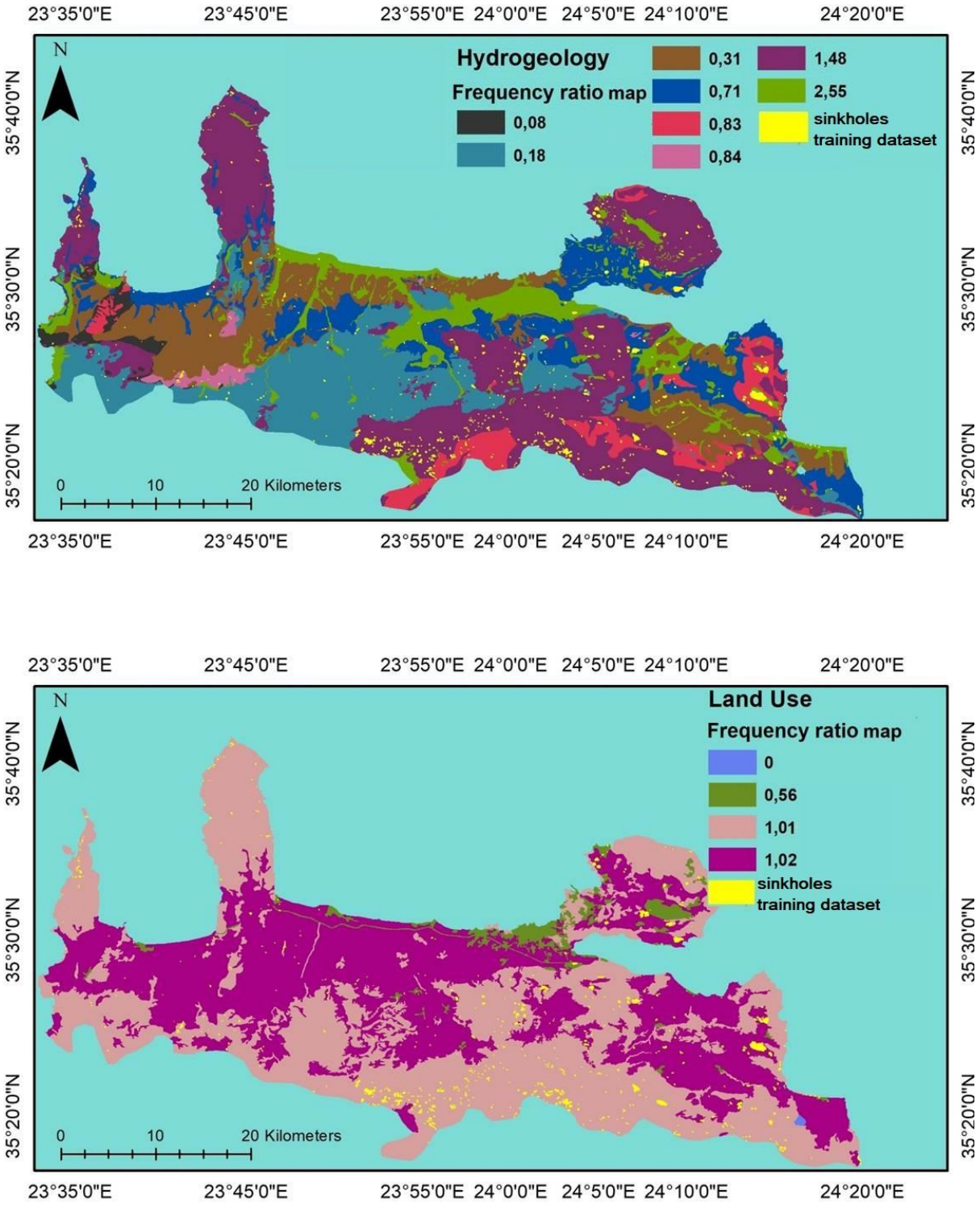

Fig.18: *Susceptibility maps of factors; hydrogeology (top) and land use (bottom)*

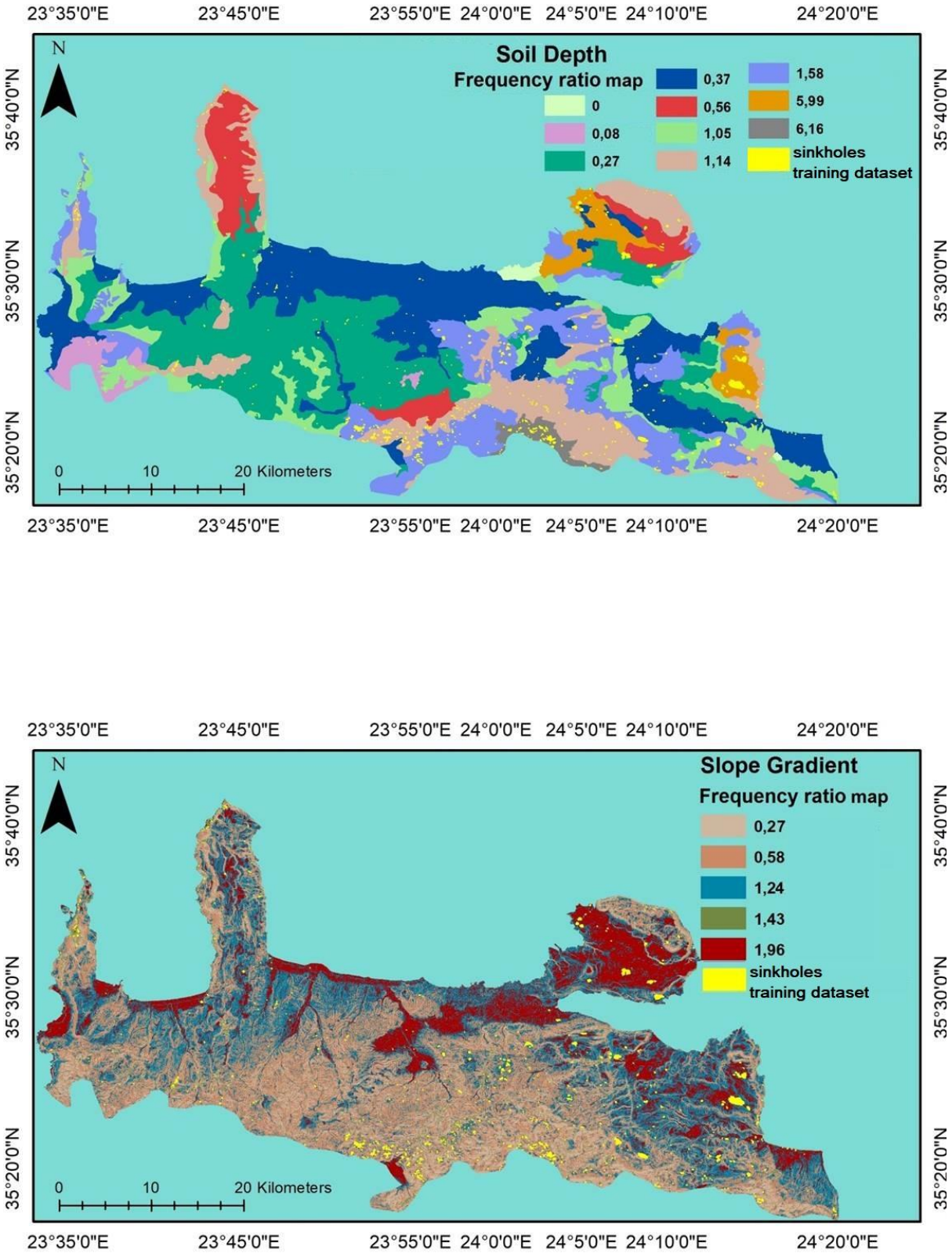

Fig.19: *Susceptibility maps of factors; soil depth (top) and slope gradient (bottom)*

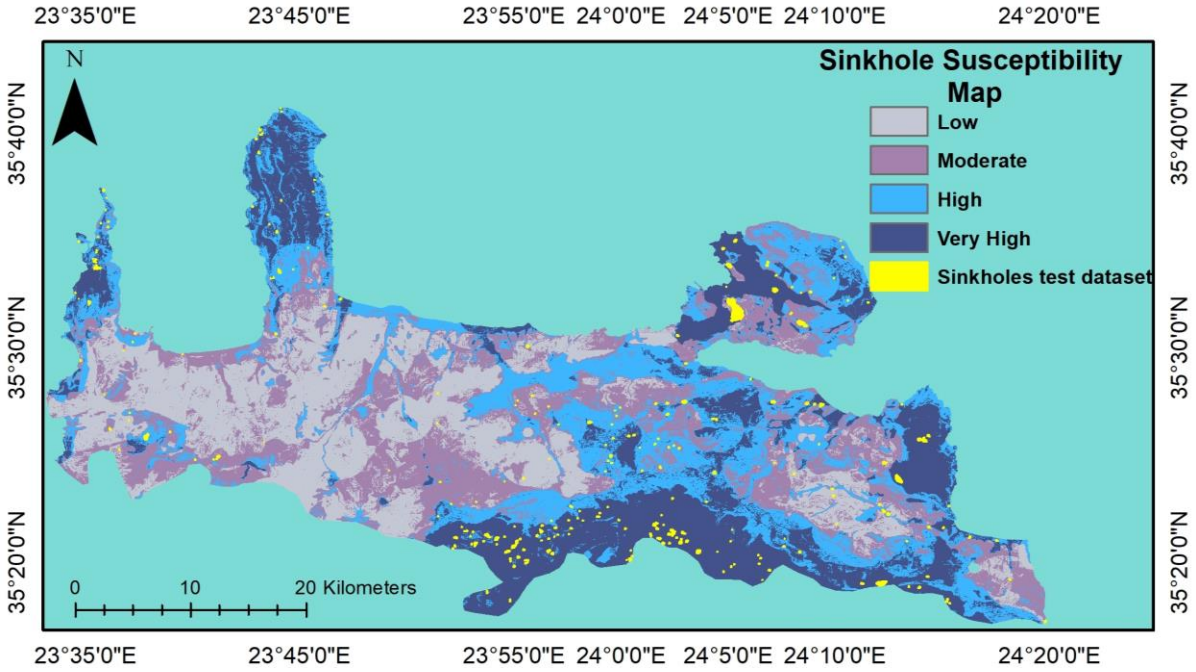

Fig.20: *Map of Sinkhole Susceptibility Index*

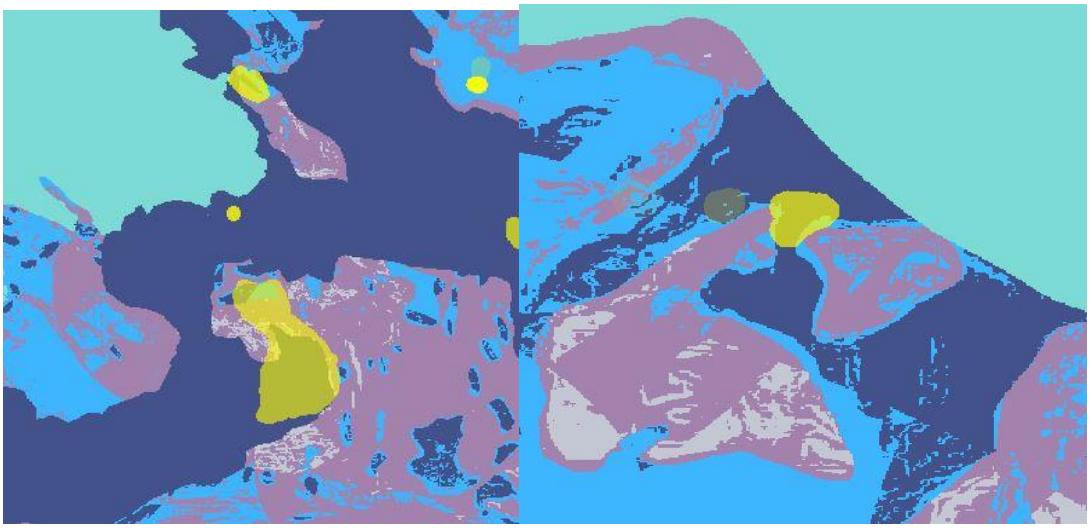

Fig.21: *Pictures that show the spatial distribution of sinkholes' test dataset with the sinkhole susceptibility map. Dark blue color refers to "very high" class.*

Some of the remaining identified sinkholes are presented below (fig.22 & fig.23), adapted by Google Earth aerial imagery. In the first image, sinkhole is filled with water and it is characterized as a small lake. This is a result of the small soil particles that have been washed down through precipitation and have blocked the "holes", lowering the hydro-permeability of the soil inside the sinkhole.

Fig. 22: *Google Earth images showing identified sinkholes in the study area*

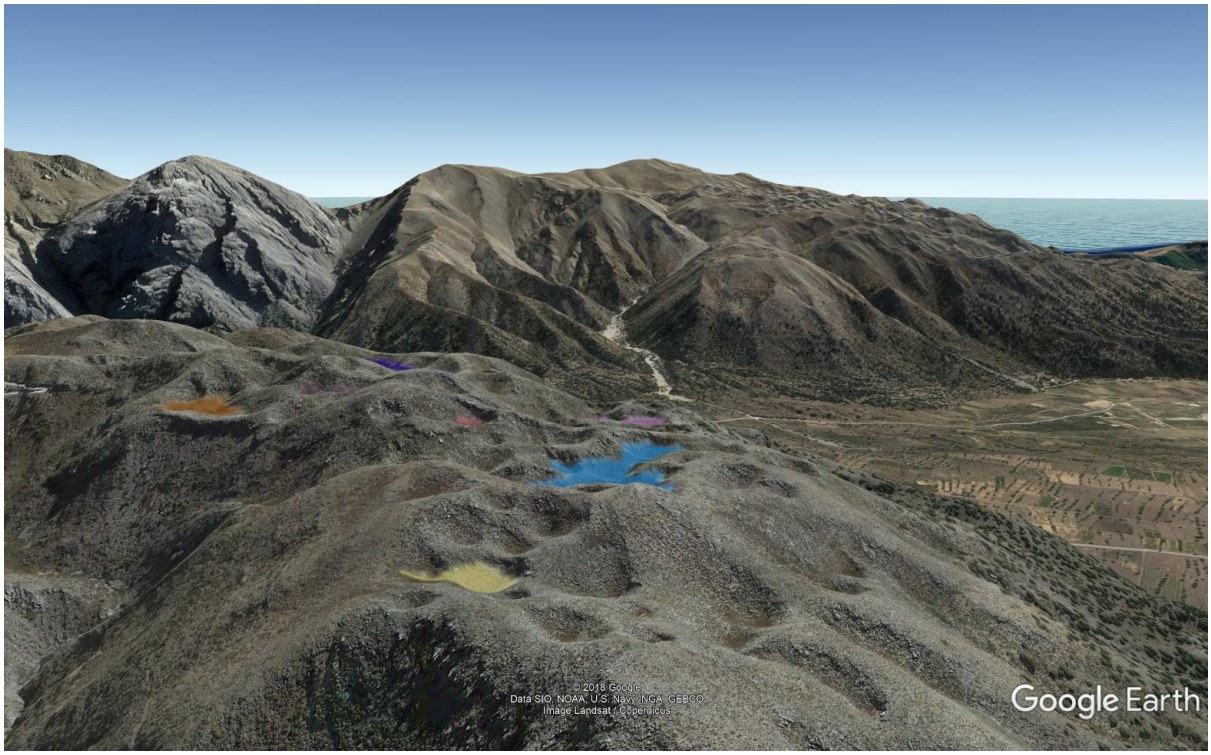

Fig.23: *Google Earth image showing sinkholes of the training dataset on Lefka Ori.*

Conclusions and proposed future research

Tandem-x has successfully mapped numerous sinkhole formations in the Northern Chania area.

After the application of various filters 1038 sinkholes were identified in 11.1-meter TanDEM-X DEM and 428 sinkholes in 30-meter TanDEM-X DEM. The second DEM identified less sinkholes due to lower spatial resolution. The constructed sinkhole inventory, including 1038 sinkholes, with morphometric data, has allowed the calculation of valuable sinkhole hazard estimates. The sinkholes were devided in the sinkhole training set dataset (70% of the total sinkholes) and the sinkhole test dataset (30% of the total sinkholes). The spatial correlation between sinkhole occurrences and groundwater pumping reveals that most of the subsidence events in the study area are induced by aquifer over-exploitation. Elevation and soil depth are the two factors that contain the classes that received the higher frequency ratios and the factor with the lowest frequency ratio class was geology's "flysch" class. The limitations of the model are partly related to the difficulty of gathering data on some relevant geological

factors, due to their hidden nature. For instance, the distribution of limestone bedrock, depth of aquifer, depth of wells and the physical parameters of groundwater would provide a more accurate result. The frequency ratio approach allowed the production of high quality model and map, in which the 83.3% of the sinkhole dataset fitted in the “high” and “very high” zones.

As a future proposed research, statistical indexes and weighting factors methods could enrich the present thesis. Machine learning algorithms, analytical hierarchy process and other geo-statistical techniques could be applied in the study area and compare them with the present study. If the available data is enough, neural networks could be tested also for sinkhole prediction analysis, since the literature on this method is very limited, but could be highly accurate.

A field study in order to characterize the physical parameters and categorize the identified sinkholes in this thesis would improve the quality of the results and would provide a better understanding of the formation mechanisms in this area.

REFERENCES

1. Nwokebuihe, Stanley Chinedu, "The description of an effective sinkhole investigation approach: a case study of two sites in Greene, County, Missouri", 2014, Masters Theses, 7267.
2. Launspach, Jonathon, 2013, Automated sinkhole extraction and morphological analysis in northeast Iowa using high-resolution LiDAR data, Electronic Theses and Dissertations. Vol. 33
3. Kenny J. A. & Hayward B. W., Karst in Stone. Karst landscapes in New Zealand: A case for protection, 2010, Geological Society of New Zealand Guidebook, Vol. 15, pp. 40
4. Gutiérrez F., Cooper A. H., Surface Morphology of Gypsum Karst, 2013, Treatise on Geomorphology Vol. 6, Karst Geomorphology
5. Chartzoulakis K.S., Paranychianakis N.V., Angelakis A.N., 2001, Water resources management in the island of Crete, Greece, with emphasis on the agricultural use Water Policy, 3, pp. 193-205
6. Nwokebuihe, Stanley Chinedu, "The description of an effective sinkhole investigation approach: a case study of two sites in Greene, County, Missouri", 2014, Masters Theses, 7267.
7. Chen Z., Auler A., Bakalowicz M., Drew D., Griger F., Hartmann J., J-iang G., Moosdorf N., Richts A., Stevanovic Z., Veni G.,& Goldscheider N., 2017, The World Karst Aquifer Mapping Project – Concept, Mapping Procedure and Map of Europe. Hydrogeology Journal, Vol. 25, pp. 771-785.
8. Adnan Ozdemir, 2015, Sinkhole Susceptibility Mapping Using a Frequency Ratio Method and GIS Technology near Karapinar, Konya-Turkey, Procedia Earth and Planetary Sciences, Vol. 15, pp. 502-506
9. Ford D., Williams P., 2007, Karst Hydrogeology and Geomorphology
10. Bouhlassa S., Fehdi Ch. & BoubayaDj., 2017, Application of Micro gravimetry to Assessing Collapse Risk in Carbonate Sinkhole Areas, Cheria Basin, Northeast of Algeria, Journal of Life Sciences, Vol. 11, pp 232-248
11. Francisco Gutiérrez, Sinkhole Hazards, 2016, Oxford Research Encyclopedia of Natural Hazard Science
12. Wadas S. H., Tanner D. C., Polom U. &Krawczyk C.M., 2017, Structural analysis of S-wave seismics around an urban sinkhole: evidence of enhanced dissolution in a strike-slip fault zone, Nat. Hazards Earth Syst. Sci., Vol. 17, pp. 2335–2350

13. Schmidt, L., 1995, Gutachtenzur hydrogeology is chen Situation Schmalkalden – unpublished report, Gesellsch. f. Ingenieur-, Hydro- und Umwelt geologie Nord hausen, pp. 1–81
14. Ravbar N., Barberá J. A., Petric M., Kogovsek J. &Andreo B., 2012, The study of hydrodynamic behaviour of a complex karst system under low-flow conditions using natural and artificial tracers (the catchment of the Unica River, SW Slovenia), Environ. Earth Sci., Vol. 65, Issue 8, pp. 2259–2272
15. Delle Rose, M. & Parise, M., 2002, Karst subsidence in South Central Apulia, Southern Italy, Int. J. Speleol., Vol. 31, pp. 181–199
16. Abelson M., Baer G., Shtivelman V., Wachs D., Raz E., Crouvi O., Kurzon I. & Yechieli Y., 2003, Collapse-sinkholes and radar interferometry reveal neotectonics concealed within the Dead Sea basin, Geophys. Res. Lett., Vol. 30, Issue 10, pp. 52.1–52.3
17. Doctor D. H., Weary D. J., Orndorff R. C., Harlow G. E., Kozar M. D. &Nelms D. L., 2008, Bedrock structural controls on the occurrence of sinkholes and springs in the northern Great Valley karst, Virginia and West Virginia, Proceedings of the 11th Multidisciplinary Conference on Sinkholes and the Engineering and Environmental Impacts of Karst, pp. 12–22
18. Del Prete S., Iovine G., Parise M.& Santo A., 2010, Origin and distribution of different types of sinkholes in the plain areas of Southern Italy, Geodinam. Ac., Vol. 23, Issue 1–3, pp. 113–127,
19. Hyland S. E., Kennedy L. M., Younos T. & Parson S., 2006, Analysis of sinkhole susceptibility and karst distribution in the northern Shenandoah valley, Virginia: Implications for low impact development (LID) site suitability models, Virginia Water Resources Research Center Special Report, Vol. 31
20. Billi A., Valle A., Brilli M., Faccenna C. & Funiciello R., 2007, Fracture-controlled fluid circulation and dissolutional weathering in sinkhole-prone carbonate rocks from central Italy, J. Struct. Geol., Vol. 29, pp. 385–395
21. Closson D. & Abou Karaki N., 2009, Salt karst and tectonics: sinkholes development along tension cracks between parallel strike slip faults, Dead Sea, Jordan, Earth Surf. Process. Landforms, Vol. 34, pp. 1408–1421
22. Farrant A. & Cooper A., 2008, Karst geohazards in the UK: the use of digital data for hazard management, Quarterly Journal of Engineering Geology and Hydrogeology, Vol. 41, pp. 339-356

23. Glade T, 2005, Linking debris-flow hazard assessments with geomorphology, Geomorphology, Vol. 66, pp. 189-213
24. Cooper AH, 2008, The GIS approach to evaporite-karst hazards in Great Britain, Environmental Geology, Vol.53, pp. 981-992.
25. Beck B., 1986, A generalized genetic framework for the development of sinkholes and Karst in Florida, U.S.A. Environmental Geology and Water Sciences, Vol. 8, Issue 2, pp. 5-18.
26. Kevin Kiernan, 2002, Forest Sinkhole Manual, Forest Practices Board, Hobart, Tasmania
27. Lei M., Gao Y., Jiang X. & Guan,(2013), Emergency investigation of extremely large sinkholes, Maohe, Guangxi, China, Proceedings of the 13th multidisciplinary conference on Sinkholes and the engineering and environmental impacts of karst, Carlsbad, pp. 293-297
28. Kent J. D.& Dunaway L., 2013, Eos, Transactions, American Geophysical Union, Vol. 94, No. 43
29. Szépszó G., Lingemann I., Klein B. &Kovács M., 2014, Impact of climate change on hydrological conditions of Rhine and Upper Danube rivers based on the results of regional climate and hydrological models. Natural Hazards., Vol. 1, pp. 241–262
30. Mulec, J. & Prelovšek. M.,2015, Freshwater biodissolution rates of limestone in the temperate climate of the Dinaric karst in Slovenia, Geomorphology., Vol. 228, pp. 787-795
31. Zhou, Y.F., Tham, L.G., Yan, R.W.M. &Xu. L., 2014, The mechanism of soil failures along cracks subjected to water infiltration, Computers and Geotechnics, Vol. 55, pp. 330-341
32. Thuringian State Institute for Environment and Geology: In genieur geologie – Baugrund – Georisiken, 2010, available at: http://www.thueringen.de/th8/tlug/uw_bericht/2011/geologie/ingenieurgeologie/
33. Geoengineer: Earth opens up in Trikala, Greece, due to erosion and karstification, 2014, available at: https://www.geoengineer.org/news/sinkholes-in-trikala-greece
34. Gordon B. L., 2013, In Defence of Uniformitarianism, Perspectives on Science and Christian Faith, Vol. 65, pp. 79-86
35. ΠΛΗΘΥΣΜΟΣΠΕΡΙΦΕΡΕΙΑΚΗΕΝΟΤΗΤΑΧΑΝΙΩΝ-1, 2011, ΕλληνικήΣτατιστικήΥπηρεσία

36. Kouli M., Loupasakis c., Soupios p., Rozos d. & Vallianatos F., 2014, Landslide susceptibility mapping by comparing the WLC and WofE multi-criteria methods in the West Crete Island, Greece, Environ Earth Sci
37. Beck B., 1986, A generalized genetic framework for the development of sinkholes and Karst in Florida, U.S.A. Environmental Geology and Water Sciences, Vol. 8, Issue 2, pp. 5-18.
38. Soupios P.M., Kouli M., Vallianatos F., Vafidis A., Stavroulakis G., 2007, Estimation of aquifer hydraulic parameters from surficial geophysical methods: A case study of Keritis Basin in Chania (Crete – Greece), Journal of Hydrology, Vol. 338, pp. 122-131
39. Kouli M., Loupasakis C., Soupios P., Rozos D., Vallianatos F., 2013, Comparing multi-criteria methods for landslide susceptibility mapping in Chania Prefecture, Crete Island, Greece, Nat. Hazards Earth Syst. Sci. Discuss., 1, pp. 73–109
40. Soupios P. M., Kalisperi D., Kanta A., Kouli M., Barsukov P., Vallianatos F., Coastal aquifer assessment based on geological and geophysical survey, northwestern Crete, Greece, 2010, Environmental Earth Sciences, Vol. 61, Issue 1, pp 63–77
41. Yalcin A., Reis S., Aydinoglu A.C., Yomralioglu T., 2011, A GIS-based study of frequency ratio, analytical hierarchy process, bivariate statistics and logistics regression methods for landslide susceptibility mapping in Trabzon, NE Turkey, Catena, Vol. 85, pp. 274-287
42. Wessel B., Huber M., Wohlfart C., Marschalk U., Kosmann D. &Roth A., 2018, Accuracy assessment of the global TanDEM-X Digital Elevation Model with GPS data, ISPRS Journal of Photogrammetry and Remote Sensing, Vol. 139, pp. 171-182
43. Hajnsek I. &Moreira A., 2006, TanDEM-X: MIssion and Science Exploration during the Phase A Study, In: Proceedings of European Conference on Synthetic Aperture Radar (EUSAR), p. 4., 16-05-2006 – 18-05-1006, Dresden Germany
44. Rahimi, M., and Alexander, E.C., Jr., 2013, Locating sinkholes in LiDAR coverage of a glacio-fluvial karst, Winona County, MN, in Land, L., Doctor, D.H., and Stephenson, J.B., eds., Proceedings of the Thirteenth Multidisciplinary Conference on Sinkholes and the Engineering and Environmental Impacts of Karst: Carlsbad, National Cave and Karst Research Institute, Symposium 2, pp. 469–480

45. Shaw Faulkner M.G., Stafford K. W. & Bryant A.W.,2013, Delineation and classification of karst depressions using LiDAR: Fort Hood military installation, Texas. In: Proceedings of the 13th Multidisciplinary Conference on Sinkholes and the Engineering and Environmental Impacts of Karst, pp. 459–468.
46. Doctor D. H., Young J.A.,2013, an evaluation of automated gis tools for delineating karst sinkholes and closed depressions from 1-meter lidar-derived digital elevation data, pp. 449-458.
47. Cahalan M. D.& Milewsk A. M., 2018, Sinkhole formation mechanisms and geostatistical-based prediction analysis in a mantled karst terrain, Catena, Vol. 165, pp. 33-344
48. Zhu J., & Pierskalla Jr. W.P., 2016, Applying a weighted random forests method to extract karst sinkholes from LiDAR data, J. Hydrol. Vol. 533, pp. 343–352
49. Douglas Ade, 2018, Quantitative Comparison of Sinkhole Geomorphology of Four Karst Regions in Ohio, The Sinkhole Conference, Multidisciplinary Conference on Sinkholes and the Engineering and Environmental Impacts of Karsts
50. Chen K.., Blong R. &Jacobson C., 2001, MCE-RISK: integrating multicriteria evaluation and GIS for risk decision–making in natural hazards, Environmental Modeling and Software, Vol. 16, pp. 387–397
51. Taheri K., Shahabi H., Chapi K., Shirzadi A.,Gutiérrez F. & KhosraviKh., 2019, Sinkhole susceptibility mapping: a comparison between Bayes-based machine learning algorithms, Land Degradation and Development
52. Burden L. I. & Todd A., 2015, A Method of Mapping Sinkhole Susceptibility Using A Geographic Information System: A Case Study for Interstates in The Karst Counties of Virginia,
53. Shirzadi A., Bui DT., Pham BT., Solaimani K., Chapi K., Kavian A., Shahabi H. & Revhaug I., 2017, Shallow landslide susceptibility assessment using a novel hybrid intelligence approach, Environmental Earth Sciences, Vol. 76, pp. 60-79
54. Ozdemir A., 2016, Sinkhole susceptibility mapping using logistic regression in Karapınar (Konya, Turkey), Bull. Eng. Geol. Environ., Vol. 75, Issue 2, pp. 681-707